



Original article

Exploring the PDE5 H-pocket by ensemble docking and structure-based design and synthesis of novel β -carboline derivativesNermin S. Ahmed^a, Amal H. Ali^a, Shreen M. El-Nashar^a, Bernard D. Gary^b, Alexandra M. Fajardo^b, Heather N. Tinsley^c, Gary A. Piazza^b, Matthias Negri^d, Ashraf H. Abadi^{a,*}^a Department of Pharmaceutical Chemistry, Faculty of Pharmacy and Biotechnology, German University in Cairo, Main Entrance, Al-Tagmoa Al-Khames, Cairo 11835, Egypt^b Drug Discovery Research Center, Mitchell Cancer Institute, University of South Alabama, 1660 Springhill Avenue, Suite 3029, Mobile, AL 36604-1405, USA^c Department of Biology, Chemistry and Mathematics, University of Montevallo, Montevallo, AL, USA^d Department of Drug Design and Optimization, Helmholtz Institute for Pharmaceutical Research Saarland (HIPS), Campus C2.3, 66123 Saarbrücken, Germany

ARTICLE INFO

Article history:

Received 11 April 2012

Received in revised form

20 September 2012

Accepted 24 September 2012

Available online 29 September 2012

Keywords:

PDE5 inhibitors

Tadalafil

Carbolines

Ensemble docking

ABSTRACT

By studying the co-crystal information of interactions between PDE5 and its inhibitors, forty new tetrahydro- β -carbolines based-analogues were synthesized, and tested for their PDE5 inhibition. Some compounds were as active as tadalafil in inhibiting PDE5 and of better selectivity profile particularly versus PDE11A, the nature of the terminal ring and its nitrogen substituent are the main determinants of selectivity. Ensemble docking confirmed the role of H-loop closed conformer in activity versus its occluded and open forms. Conformational studies showed the effect of bulkiness of the terminal ring N-alkyl substituent on the formation of stable enzyme ligands conformers. The difference in potencies of hydantoin and piperazinedione analogues, together with the necessity of C-5/C-6 R-absolute configuration has been revealed through molecular docking.

© 2012 Elsevier Masson SAS. All rights reserved.

1. Introduction

The cyclic nucleotides adenosine monophosphate (cAMP) and cyclic guanosine monophosphate (cGMP) play important regulatory roles in signal transduction processes. cGMP is recognized as a second messenger for atrial natriuretic peptide and nitric oxide signalling resulting in the relaxation of blood vessels [1,2]. Phosphodiesterase (PDE) enzymes play an important regulatory role in both the cAMP and cGMP transduction processes through degradation of these second messengers to the corresponding mononucleotides, adenosine monophosphate and guanosine monophosphate [3–5]. The PDE superfamily consists of 11 family members, coded for by 21 genes with multiple splice variants. PDE4, PDE7 and PDE8 specifically hydrolyze cAMP; PDE5, PDE6 and PDE9 are cGMP specific, whilst PDE1, PDE2, PDE 3, PDE10 and PDE11 show dual specificity and hydrolyze both nucleotides. PDE5 is widely distributed, throughout the body, being found in smooth muscle throughout the body and also found in platelets and lung [6–8]. This has led to the approval of sildenafil and tadalafil for the

treatment of MED and pulmonary hypertension [9,10]. Ongoing clinical studies with PDE5 inhibitors have highlighted the potential use of PDE5 inhibitors in range of additional indications such as cardioprotection [11], enhancement of memory and cognitive functions [12] and the treatment of diabetic peripheral neuropathy [13]. Also, recent studies suggest their possible therapeutic application of PDE5 inhibitors in cancer therapy [14,15].

The high degree of similarity within the PDE enzyme family [16] is the main reason for selectivity issues affecting many known PDE5 inhibitors. The active site of PDE5 is placed in the center of the C-terminal helical bundle domain and it includes five subsites: while the metal-binding site (M site) and the core pocket (Q-pocket; lined by Gln817, Phe820, Val782, Tyr612) are common to most of the PDE family members, the hydrophobic pocket (H-pocket), the Q₂-pocket (lined by Phe786, Phe787, Leu804, Ile813, Met816) and the lid region (L region) show significant differences with respect to other PDE [17–19]. Therefore targeting at least one of these last three regions represents a promising strategy to reduce the promiscuity affecting many PDE5 inhibitors.

Several crystal structures of PDE5 exist, either co-crystallized with different inhibitors or substrates or as apoform (Table S11). Interestingly, they present the largest structural diversity in the characteristic regions of PDE5, in particular in the H-loop (residues

* Corresponding author. Tel.: +20 227590716; fax: +20 227581041.

E-mail address: ashraf.abadi@guc.edu.eg (A.H. Abadi).

660–683) and the M-loop (residues 788–811) [20]. H-loop and M-loop are often not resolved at all or, alternatively, they are mutated into chimeric PDE5/PDE4 or PDE5/PDE6 hybrid forms (Table S11). Remarkably, the conformational ensemble exists not only by virtue of the presence of different ligands, but also with the very same inhibitor. This suggests for PDE5 the existence of a multitude of metastable states and that approaching ligands will bind into pre-existing PDE5 conformations following a selected-fit mechanism. However, this also means that a larger sampling of the conformational space of PDE5 might be required for the search of the “correct” PDE5 conformer to best reproduce binding mode and structure–activity relationships at least within one inhibitor series.

In the two crystal structures with tadalafil **I** the H-loop is either only partially resolved (PDB 1UDU [19]; dimer form; residues I665–L675 are missing) or it is replaced by the PDE4 counterpart (PDB 1XOZ [18]; chimeric PDE5-PDE4_{H-loop} construct). In the chimeric crystal 1XOZ the H-loop assumes a bi-helical conformation with access to the binding site widely open. In 1UDU, on the contrary, the H-loop is resolved only until Tyr664, but with the existing segment supportive of the existence of a closed-conformer as highlighted by the close proximity of the N-Met group of tadalafil within 4 Å of the backbone of Asn662-Ser663-Tyr664.

Tadalafil is mainly stabilized by a single monodentate hydrogen bond with Gln817 and by π -stacking with the hydrophobic p-clamp forming residues Phe820 and Val782 as well as with the Q₂-pocket lining Phe786 and Leu804. Point mutations confirmed the importance of these interactions, but also suggested an important role in tadalafil binding to His613 and Tyr612 [21]. On the contrary no clear interaction pattern could be determined for the piperazinedione ring and its N-methyl substituent due to the conformational variability of the H-loop. As most of the β -carboline derivatives reported in the last years bear structural variations in this region of **I** [9,10,22–26], it is important to solve the role played by the H-loop in inhibitor binding to further improve the drug design.

The aim of this study was the development of a series of novel β -carboline derivatives, the elucidation of their binding mode and their preference for the PDE5 conformation. A particular focus was set on the investigation of different H-loop conformers as well as on the identification of the best PDE5 conformer best resembling the structure–activity profile for this class of inhibitors. Thereby, we combined molecular modelling with chemical synthesis and biological evaluation. Results of a first ensemble docking with a small

set of inhibitors (**1**, **29**, **30**) indicated the occluded/closed conformer as the most appropriate to resemble the binding behaviour of these inhibitor-series, but also as capable to host larger N-alkyl chains.

Due to these results our laboratory designed a novel compound series which maintains the tetracyclic- β -carboline moiety of compound **I** and its active analogues **II–IV** (Table 1) [23–25], but replaced the pendant benzodioxole of **I** with a 4-bromophenyl ring in order to exploit the PDE5 characteristic Q₂-pocket in terms of activity and selectivity. Further, we exploited the stereoisomers and varied the N-alkyl substituents on both hydantoin and piperazinedione rings in length, branching, and bulkiness (ethyl, butyl, *sec*-butyl and *tert*-butyl instead of methyl). Finally, we retrospectively analyzed an enlarged set of inhibitors in multiple single-conformer docking runs with Autodock Vina with the N-alkyl substituents acting as probes in the exploration of H-loop and L-loop regions. This allowed insights into the influence of H-loop on the inhibitory potency, the identification of the closed PDE5 conformer as the preferred one for binding of the β -carbolines, notably in agreement with the folding of the PDE5-**I** co-crystal 1UDU, and finally the determination of two stereospecific binding modes, one for 5/6R and one for 5/6S-derivatives.

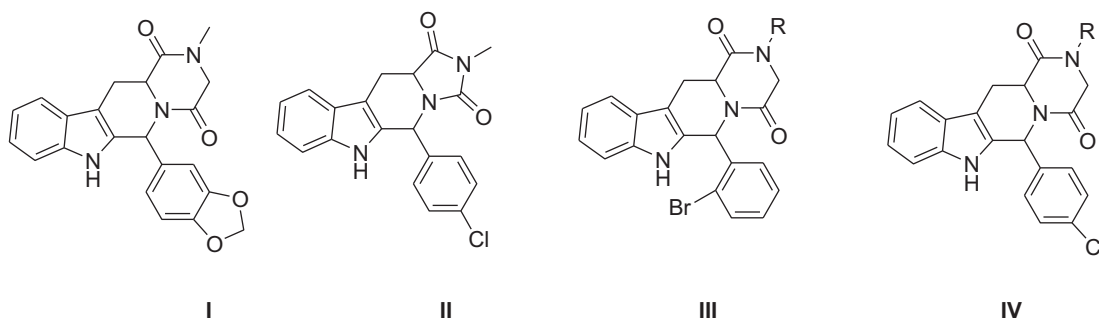
2. Results

2.1. Chemistry

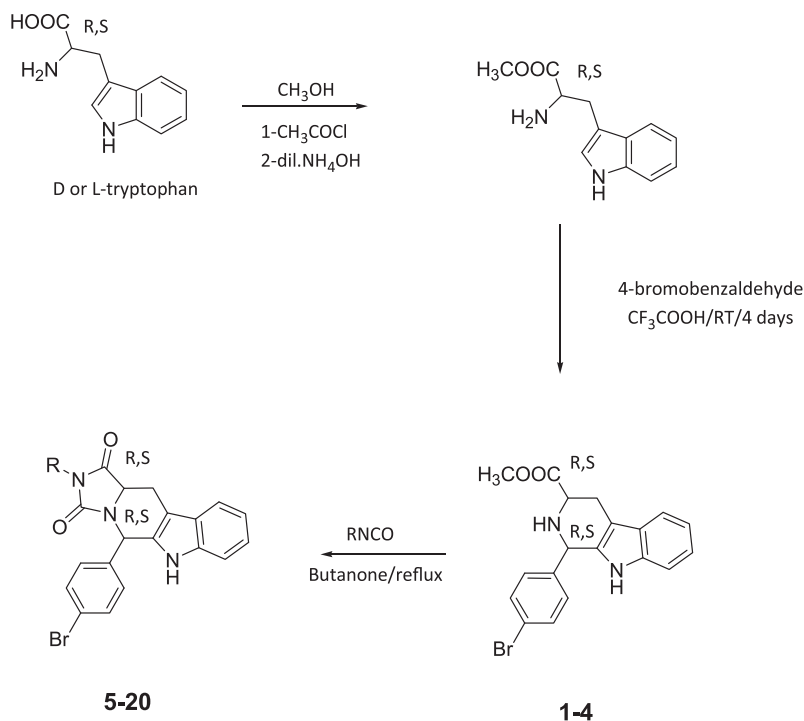
The general synthesis of hydantoin compounds are depicted in Schemes 1 and 2. Pure D- or L-tryptophan methyl ester [24] and *p*-bromobenzaldehyde were subjected to a Pictet–Spengler reaction. Since we initially desired access to both the *cis*- and *trans*-isomers (**1–4**), the reaction was carried under non stereospecific conditions. The *cis*- and *trans*-1,3-disubstituted tetrahydro- β -carbolines (**1–4**) were separated by column chromatography, each of the pure diastereomers was allowed to react with commercially available isocyanates to yield the desired *cis*- and *trans*-hydantoin.

Piperazinedione derivatives were prepared by the chloroacetylation of pure *cis*- and *trans*-1,3-disubstituted tetrahydro- β -carbolines (**1–4**) in the presence of NaHCO₃. This step provided the respective chloroethanone derivative in an excellent yield. The piperazinedione diastereomers were then obtained by ring closure of the corresponding chloroacetyl derivatives in the presence of primary amines, namely ethylamine and *tert*-butylamine.

Table 1
% Inhibition and IC₅₀ values of tadalafil and some analogues.



Code	R	Absolute stereo-chemistry	% PDE5 inhibition at 10 μ M	IC ₅₀ μ M
I	Methyl	(6R,12aR)	100	0.003
II	Ethyl	(5R,11aR)	85	1.1
III	Ethyl	(6R, 12aR)	98	0.32
IV	Ethyl	(6R,12aR)	105	0.003



Compound	R
5-8	ethyl
9-12	butyl
13-16	sec-butyl
17-20	tert-butyl

For the exact stereochemistry of compounds **1-20**, see experimental

Scheme 1. Synthesis of hydantoin series.

The assignment of *cis*–/*trans*–stereochemistry for the tetrahydro- β -carbolines (**1-4**) was based on detailed study of ^{13}C NMR spectroscopy data as established from previous studies [9,22]. Signals for C-1 and C-3 in the *trans*-isomers appear at higher field in the carbon spectrum than the analogous carbons of the corresponding *cis*-isomer, probably due to the 1, 3-interactions present in the *trans*-tetrahydro- β -carboline isomer. The ^1H NMR signals for the proton at C-1, of the 1,3-disubstituted-tetrahydro- β -carbolines (**1-4**) appeared at about δ 5.20–5.35 ppm, a remarkable downfield shift is noticed upon cyclization to the hydantoin and piperazinedione derivatives, the introduced carbonyl group deshields the same proton which is now attached to C-5 and C-6, respectively.

Notably, regarding the tetrahydro- β -carbolines a significant difference has been noted between the 2 isomers regarding their R_f values. A correlation exists between R_f value on TLC and the stereochemistry of the 1, 3-disubstituted tetrahydro- β -carbolines. The *cis*-isomer is systematically less polar than the *trans*-isomer; however, in the hydantoin series, the polarity is reversed, thus, the *cis*-isomer becomes more polar than the *trans*-isomer. The

difference in R_f values are not as significant in the piperazinedione series as it is in the hydantoin series. In mass spectrometry, the molecular ion peaks appeared at M^+ and $M^+ + 2$ due to the isotopic nature of the bromine atom.

2.2. Molecular modelling

2.2.1. Structural analysis

All crystal structures of PDE5 were retrieved from the PDB database [27] and superimposed using software package MOE (MOE 2010.10; Molecular Operating Environment; <http://www.chemcomp.com>) with PDB 2H42 (chain A) [20] as reference structure. Only two out of twenty-three crystal structures are fully solved and with wild-type sequence (PDB 2H42, 2H44). Therefore, the PDE5 crystals were clustered using the Consensus module of MOE including only those with a resolved H-loop and with sequence variability as additional criterion (i.e. PDE5, PDE4 and PDE6). Clustering with an RMSD cut-off >1 Å yielded into three

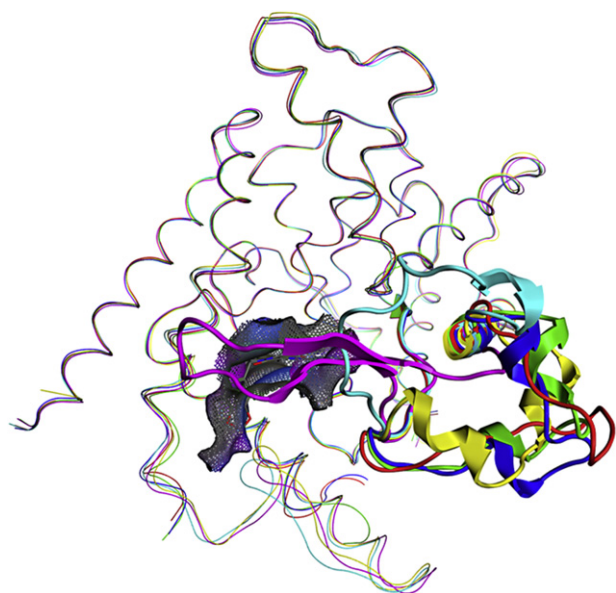


Fig. 1. Superimposition of PDE5 structures resembling six distinct H-loop conformers. H-loops are rendered as cartoons (PDB 1RKP green, 3BJC blue, 1XOZ yellow, 2H40 red, 2H42 cyan, 2H44 magenta) whereas the rest of the PDE5 structure as thin ribbons. The surface of the binding pocket of tadalafil is shown as lines. (For interpretation of the references to colour in this figure legend, the reader is referred to the web version of this article.)

pendant benzodioxole of **1** and the Q₂-pocket lining residues Ala783, Phe786, Phe787, Leu804, Ile813 and Met816 as well as between the β -carboline moiety and Tyr612, Leu765, Ala767, Ile768, Val782, Gln775, Ile778 and Ala779; 4) water-mediated hydrogen bond with His613/Asn661, residues involved in metal ions ligation (Zn^{2+} and Mg^{2+}).

2.2.2. Ensemble docking

For these studies there was a need to identify which PDE5 conformer best reflects the binding behaviour of tadalafil and congeners. Based on the results of the Consensus Scoring our conformational ensemble was built including four most representative structures, namely PDB 2H44 (closed) [20], 2H42 (occluded) [20], 3BJC [16] and 1XOZ (open) [19]. For the open state two structures were included in order to consider both the wild type form (3BJC) as well as the original tadalafil co-crystal structure (1XOZ), which is a hybrid form. As 3BJC lacks part of the M-loop a homology model using the M-loop of 2H42 as template was built. This PDE5 conformer collection was explored with a small sub-set of inhibitors in an ensemble docking using GOLDv5.0 with GOLD-SCORE (GS) [33,34] fitness function. The inhibitor set comprised compound **1** (with known IC₅₀), and the newly designed **29** and **30**, which differ in stereochemistry. According to the GS scoring values and the number of poses found per conformer a preference for the closed (2H44)/occluded (2H42) crystals emerged for compound **29**, whereas for **1** no clear preference could be determined with the poses equally divided in open (1XOZ) and occluded (2H42) conformers. Conversely, for the 6S-isomer **30** a clear preference for the open conformers resulted, with the N-alkyl substituent pointing into the buried wall of the Q-pocket (Table S12).

2.2.3. Multiple single-conformer docking

In order to validate the results of the ensemble approach on a larger dataset and to retrospectively derive a precise structure–activity relationships for this inhibitor class we performed a multiple single conformer docking with AutoDock Vina v.1.1.2 was

performed [35] The number of compounds were increased up to twenty-five, taking care to include different stereoisomers with N-alkyl substituents of different length, shape and size, and docked them in each of the four PDE5 conformers used in the ensemble. Plotting the predicted binding affinities of the top ranked pose of each compound against the pIC₅₀ values resulted in the closed conformer (2H44, $r = 0.83$; Fig. 2) clearly outperforming the open (1XOZ, $r = 0.52$, 3BJC, $r = 0.40$) and the occluded (2H42, $r = 0.51$) (Fig. S11) conformers both in terms of affinity prediction and discrimination between potent and inactive/weak inhibitors.

2.3. Biology

Compounds were evaluated in an *in vitro* assay for inhibitory activity against human PDE5; each compound was evaluated in two steps. The first step was the determination of the percentage of inhibition at 10 μ M performed in triplicate. For compounds displaying a percentage of inhibition greater than 60%, the IC₅₀ was determined from a concentration–response curve using a range of 8 concentrations (1 nM–10 μ M) with at least two replicates per concentration. The results are shown in Tables 2–5. Moreover, for compound **8**, **25**, **28**, **29** and **33** the selectivity towards other PDEs (PDE1A, PDE2A, PDE3A, PDE3B, PDE9A, PDE10A and PDE11A) were evaluated at a concentration of 50 μ M, the results are shown in Table 6. For compounds that displayed greater than 50% inhibition, IC₅₀ values were determined.

3. Discussion

Ensemble docking of multiple protein structures has proven successful as tool in drug design and enzyme dynamics issues [28–32]. The strong advantages of this method are the inclusion of protein plasticity and the significantly reduced risk of inadvertently choosing an unsuitable protein model. Further an ensemble consisting of a reduced yet significant amount of conformations is often enough to improve the docking performance [33]. This study systematically investigated the effect of different N-alkyl substituents on their inhibitory potency, making use of four representative PDE5 conformations.

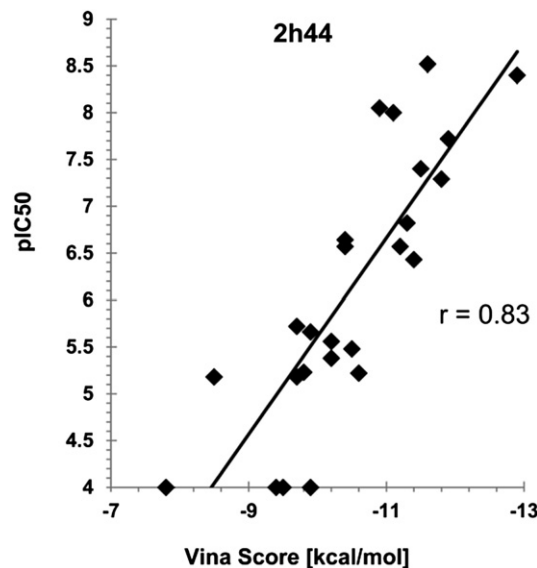
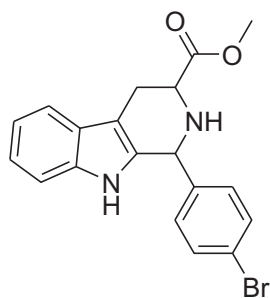


Fig. 2. Binding affinities (in kcal/mol) plotted versus the pIC₅₀ of 25 compounds as output of the closed PDE5 conformer docking run with AutoDock Vina 1.1.2 with the regression coefficient r .

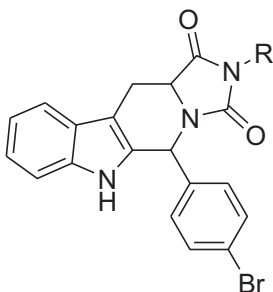
Table 2
% Inhibition and IC₅₀ values for tetrahydro-β-carbolines.



Code	Absolute stereo-chemistry	% PDE5 inhibition at 10 μM	IC ₅₀ μM
1	(1R,3R)	10	ND*
2	(1S,3R)	10	ND
3	(1S,3S)	17	ND
4	(1R,3S)	75	4.2

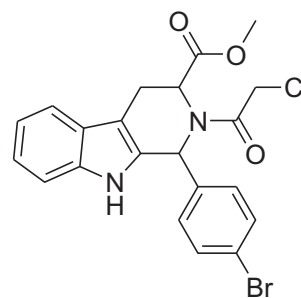
The introduction of a 4-bromophenyl instead of the pendant benzodioxole ring of compound **I** was guided by several considerations: first, the size of Q₂-pocket strongly diverges within the PDE family making it an ideal targeting for improved selectivity and potency of novel inhibitors; second, as bromine is an isostere of chlorine and as the activity of compound **IV** (*p*-chlorophenyl) is almost 100 times the activity of the *o*-bromine analogue **III**, studying the impact of positional isomerism is of great importance; third, bromine is bulkier and more lipophilic than chlorine and may fill the prevalently lipophilic Q₂-pocket. In fact, potent compounds were obtained as evidenced by the compound **29** (IC₅₀ = 3 nM),

Table 3
% Inhibition and IC₅₀ values for hydantoin derivatives.



Code	R	Absolute stereo-chemistry	% PDE5 inhibition at 10 μM	IC ₅₀ μM
5	Ethyl	(5R,11aR)	94.4	2.8
6	Ethyl	(5S,11aR)	89.3	3.9
7	Ethyl	(5S,11aS)	79.8	>10
8	Ethyl	(5R,11aS)	100.9	0.051
9	Butyl	(5R,11aR)	98.7	0.230
10	Butyl	(5S,11aR)	72.1	>10
11	Butyl	(5S,11aS)	81.5	>10
12	Butyl	(5R,11aS)	106.0	0.04
13	<i>sec</i> -Butyl	(5R,11aR)	83	0.37
14	<i>sec</i> -Butyl	(5S,11aR)	67	6.0
15	<i>sec</i> -Butyl	(5S,11aS)	72	3.3
16	<i>sec</i> -Butyl	(5R,11aS)	92	0.15
17	<i>tert</i> -Butyl	(5R,11aR)	91	0.27
18	<i>tert</i> -Butyl	(5S,11aR)	78	2.2
19	<i>tert</i> -Butyl	(5S,11aS)	38	ND
20	<i>tert</i> -Butyl	(5R,11aS)	94	0.27

Table 4
% Inhibition and IC₅₀ values for chloroethanone derivatives.

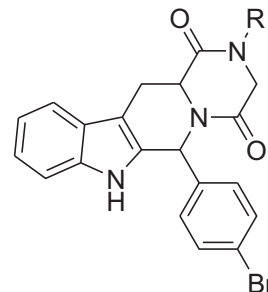


Code	Absolute stereo-chemistry	% PDE5 inhibition at 10 μM	IC ₅₀ (μM)
21	(1R,3R)	25	>10
22	(1S,3R)	17	>10
23	(1S,3S)	19	>10
24	(1R,3S)	21	>10

which is as active as tadalafil **I** and analogue **IV** outperforming the *o*-bromophenyl analogue **III** (IC₅₀ = 320 nM).

All short tetrahydro-β-carboline derivatives (**1–4**; **21–24**), with the exception of compound **4** (IC₅₀ = 4.2 μM), possess no PDE5 inhibitory activity indicating the crucial need for a fused tetracyclic ring. Introduction of carbonyls is not sufficient to yield inhibition suggesting that a rigidification of the carbonyls must occur in order to interact via water-bridging with His613 and with the backbone carbonyl of Met816 as seen for **I** in 1XOZ [21,36]. Still, given an appropriate stereochemistry (i.e. **4** – 1R,3S) some potency might be

Table 5
% Inhibition and IC₅₀ values for piperazinedione derivatives.



Code	R	Absolute stereo-chemistry	% PDE5 inhibition at 10 μM	IC ₅₀ μM
25	Methyl	(6R,12aR)	98	0.019
26	Methyl	(6S,12aR)	94	6.6
27	Methyl	(6S,12aS)	87	1.9
28	Methyl	(6R,12aS)	91	0.012
29	Ethyl	(6R,12aR)	96	0.003
30	Ethyl	(6S,12aR)	97.9	1.9
31	Ethyl	(6S,12aS)	83	0.22
32	Ethyl	(6R,12aS)	98.7	<0.01
33	Butyl	(6R,12aR)	87	0.009
34	Butyl	(6S,12aR)	81.5	6.6
35	Butyl	(6S,12aS)	80	5.9
36	Butyl	(6R,12aS)	92	0.01
37	<i>tert</i> -Butyl	(6R,12aR)	30	ND
38	<i>tert</i> -Butyl	(6S,12aR)	27	ND
39	<i>tert</i> -Butyl	(6S,12aS)	12	ND
40	<i>tert</i> -Butyl	(6R,12aS)	21	ND

Table 6
IC₅₀ (μM) of compound **25** and tadalafil versus an array of PDEs.

Cpd	PDE1A inhibition		PDE2A inhibition		PDE3A inhibition		PDE3B inhibition		PDE5A inhibition	PDE9A inhibition	PDE10A inhibition		PDE11A inhibition	
	IC ₅₀ μM		IC ₅₀ μM		IC ₅₀ μM		IC ₅₀ μM		IC ₅₀ μM	IC ₅₀ μM	IC ₅₀ μM		IC ₅₀ μM	
	cAMP	cGMP	cAMP	cGMP	cAMP	cGMP	cAMP	cGMP	cGMP	cGMP	cAMP	cGMP	cAMP	cGMP
1	>50	>50	>50	>50	>50	>50	>50	>50	0.003	>50	>50	>50	0.295	0.05
8	>50	>50	>50	>50	>50	>50	>50	>50	0.051	>50	>50	>50	44.00	35.70
25	>50	>50	>50	>50	>50	>50	>50	>50	0.019	>50	>50	41.7	0.6	0.270
28	>50	>50	>50	>50	>50	>50	>50	>50	0.012	>50	>50	>50	1.30	1.13
29	>50	>50	>50	>50	>50	>50	>50	>50	0.003	>50	26.1	14.7	0.30	0.27
33	>50	>50	>50	>50	>50	>50	>50	>50	0.009	>50	>50	>50	1.20	0.60

retained with the β-carboline moiety being able to form a hydrogen bond with Gln817 and π-stacking with the P-clamp residue Val782 (Phe820 as well), eventually reinforced by cation–π interactions between the protonated secondary amine (protonation state at pH 7 predicted with MOE) and Phe786, as suggested by docking poses (Fig. S13). This hypothesis is strengthened by the fact the insertion of a chloroethanone group on the nitrogen depletes all inhibitory potency.

3.1. 5/6 R-isomers

The best scored docking poses of the 5/6 R derivatives all resemble the crystallographic binding mode of **1** and its interactions with the Q-pocket, P-clamp and Q₂-pocket residues. Accordingly, the reasons for the marked differences in terms of potency have to be identified in the final five or six membered rings and their N-alkyl substituents. The last consideration fits also for the 5/6 S analogues, albeit in that case the residues involved in favourable or repulsive interactions are placed on the opposite and buried part of the Q-pocket.

The most active 5R-hydantoin analogue is **12** (IC₅₀ = 40 nM) bearing an *n*-butyl group, whereas the most active piperazinedione analogue **29** (IC₅₀ = 3 nM) has an ethyl on the N. Flexible and non-branched rather than bulky and rigid alkyl chains seems to ensure a higher potency [24]. For the hydantoin series the activity increases with the length (*n*-butyl > ethyl), whereas for the piperazinediones ethyl was the best substituent followed by *n*-butyl and methyl. For both series the activity decreases with the bulkiness (*n*-Bu > *sec*-Bu > *tert*-Bu) of the N-substituent, with stronger effects for the piperazinediones, whereas a *tert*-butyl (**37–40**) depletes the inhibitory potency in contrast to their hydantoin analogues.

However, comparing hydantoin and piperazinedione congeners the length of the N-alkyl chain seems to play a subordinated role compared to the size of the fused ring, as evidenced by the 1000 times improved activity of the six member ring compound **29** compared to its five member congener **5** (IC₅₀ of 3 and 2800 nM, respectively). As seen in the docking poses (Fig. 3) this might be due to the facts that while **29** can interact with both the crystallographic waters (and thus with His613 and Met816), the small hydantoin ring of **5** can only catch one water molecule. Furthermore, the methylene at the bridgehead between the two nitrogen atoms in **29**, missing in the hydantoin series, is close to the L-region residues Ile665, Leu725, Leu804 and Met816 ensuring a better anchoring inside the binding pocket in virtue of favourable van der Waals interactions. The N on the terminal piperazinedione ring placed closer to the H-loop (Fig. 4) explains the diverse SAR observed for the R substituent in the two series, in particular the preference for *n*-butyl (**12**) and ethyl (**29**) as well as the moderate potency of *tert*-butyl (**20**; IC₅₀ 0.27 μM) versus an IC₅₀ more than IC₅₀ > 10 μM (**37**).

Leu804 is placed at the top of a 3.10 helix within the M-loop in close vicinity to the H-loop residues S663-Y664. Here it forms the

outer wall of the Q₂-pocket, delimiting it and contributing to narrow the access path to the binding site. H-loop and M-loop are the most flexible regions of the enzyme and both are partially not resolved in the PDE5 crystal ensemble. Considering the labile nature of the M-loop 3.10 helix it is possible that its unfolding could affect both the M-loop and the tightly interconnected H-loop [37], thus eventually leading to solvent exposure of the Q-pocket.

3.2. 5/6 S-isomers

All 5/6 S derivatives were docked rotated of 180° compared to the 5/6 R isomers with the N-alkyl pointing towards the buried Q-pocket with the 4-bromophenyl ring fitted into the Q₂-pocket. Among the most potent analogues with C5/6 are of the S configuration (**18, 30**), they are stabilized by hydrogen bonds with Gln817 via one of their carbonyl oxygen on the terminal ring and π-stacking with the P-clamp residue Phe820 (Fig. 5). The alkyl groups, such as *tert*-butyl in the hydantoin derivative **18** and ethyl in the piperazinedione derivatives **30** and **31**, are buried in a hydrophobic pocket formed by Tyr612, Leu765, Ala767, Ile768, Gln775, Ile778 and Val782, but their stabilization is strongly dependent on size, and bulkiness otherwise it results in severe steric clashes. The carboline moiety is placed into the H-pocket, where it interacts via π-stacking with Phe786 and van der Waals interactions with Ser663, Ile665, Leu725 and His613. Notably, in this pose the carboline would displace the important water molecule linking **1** with His613 thus explaining (paired with the stringent requirements for the *n*-alkyl substituent) the overall weaker inhibitory potency of the 5/6 S isomers with respect to their 5/6 R congeners.

The close vicinity of the N-alkyl groups to the H-loop residues Asn661, Ser663 and Ile665 (H-loop) for the 5/6 R-isomers as well as to Tyr612 and Gln775 for the 5/6 S-isomers suggests that replacing the N-alkyl group with polar acceptor atoms containing groups or with halogen atoms in analogy to the recent study of Xu et al. [38], might lead to novel β-carboline derivatives with improved potency and selectivity.

3.3. Selectivity

Compounds **8, 25, 28, 29** and **33** showed inhibitory activities versus PDE5 and PDE11 with cGMP as the substrate with selectivity profiles of 700, 14, 94, 90, and 67, respectively (Table 6). Interestingly, four out of the five compounds showed selectivity profile better than tadalafil (selectivity index; 17). Increasing the bulkiness of the terminal ring N-alkyl substituent and reducing the size of the terminal ring are the main determinant favouring selectivity. Since these N-alkyl substituents are involved in hydrophobic interaction with ILE665 of the H-loop, thus, it seems that there are crucial differences between PDE5 and PDE11 in the size and nature of the residues in those particular corresponding pockets.

Differences in the selectivity of **8** versus **25** may also indicate differences in the occurrence of water molecules in the pocket.

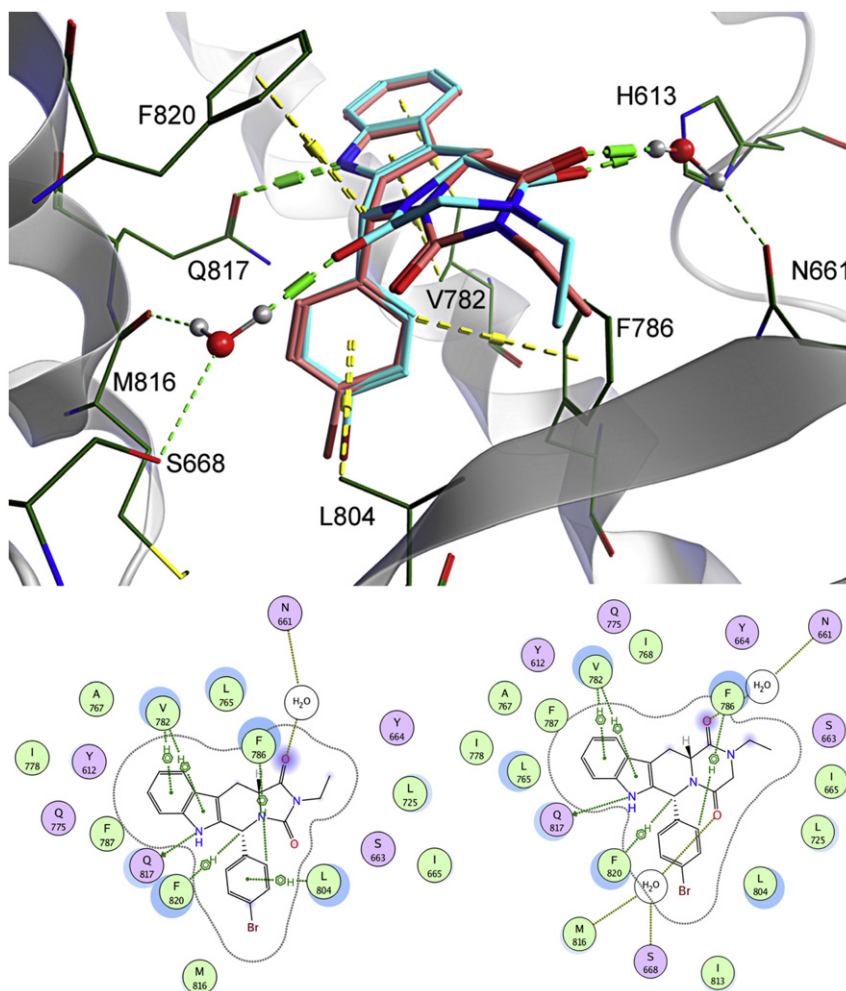


Fig. 3. Binding modes of compounds **5** (rosa) and **29** (cyan). The reduced size of the hydantoin ring of **5** allows interaction with only one water molecule (sphere representation) in contrast to **29**, which is more tightly anchored into the active side by two water-mediated bridges with His613/Asn661 and Met816. H-bonds are rendered as green dots, whereas CH- π and other π -stacking interactions as yellow ones. In the two 2D-ligand-PDE5 interactions plots hydrophobic/aromatic residues are coloured in green, whereas polar amino acids in magenta. H-bonds and all π -stacking interactions are shown as green dotted lines, whereas intra-residue interactions in green-yellow. The active site contour is also shown. (For interpretation of the references to colour in this figure legend, the reader is referred to the web version of this article.)

4. Conclusion

In this study, a novel series of hydantoin and piperazinedione β -carboline were presented as selective PDE5 inhibitors. Via ensemble docking the effects of different N-alkyl substituents as well as of different stereoisomers on PDE5 inhibition were tested. For these inhibitor series a preference for the closed/occluded PDE5 conformer was determined, which closely resembled the existing part of the truncated PDE5-compound **I** co-crystal complex 1UDU. Furthermore, an appreciable correlation between the predicted binding affinity and the pIC_{50} values of the investigated compounds was observed for the closed conformer, whereas with the open conformer there was no distinction between potent and inactive compounds. Finally, we could show the necessity of *R*-absolute configuration at C-5 and C-6 was demonstrated and regardless to the absolute configuration at C-11a and C-12, and the existence of two stereospecific binding modes for 5/*6R* and 5/*6S*-isomers, respectively.

The largest differences in potency prediction were observed for the *n*-butyl-piperazinedione series which were all underestimated. This leads to the conclusion that the closed/occluded conformer still might not be adequate and further conformational studies of the diverse H-loop conformers and the importance of Ile665, Leu804 and Met816 sites need to be further investigated to fully

disclose the modulating effects of N-alkyl substituents on the inhibitory potency.

Compounds with high activity and selectivity profile towards cGMP PDE5 versus cGMP PDE11 were obtained e.g. **8**, **28**, **29**, and **33**. Thus, carbolines with different terminal rings and different terminal N-substituents might be proposed to modulate selectivity. Although the catalytic domain is highly conserved between PDE5 and PDE11 the functional role of PDE11 is controversial therefore the identification of selective PDE5 analogues is required. Future design of PDE5 inhibitors should consider the use of variable polar N-substituents rather than the classical non-polar alkyl groups this modification would reveal novel H-loop interactions which potentially could enhance potency and selectivity of novel inhibitors.

5. Experimental

5.1. Chemistry

All starting materials were commercially available and of pure analytical grade. All reactions were carried out under inert gas (nitrogen). Organic extracts were dried over anhydrous Na_2SO_4 . Solvents were removed under reduced pressure using a rotavap. Reaction progress was monitored by TLC, performed on precoated

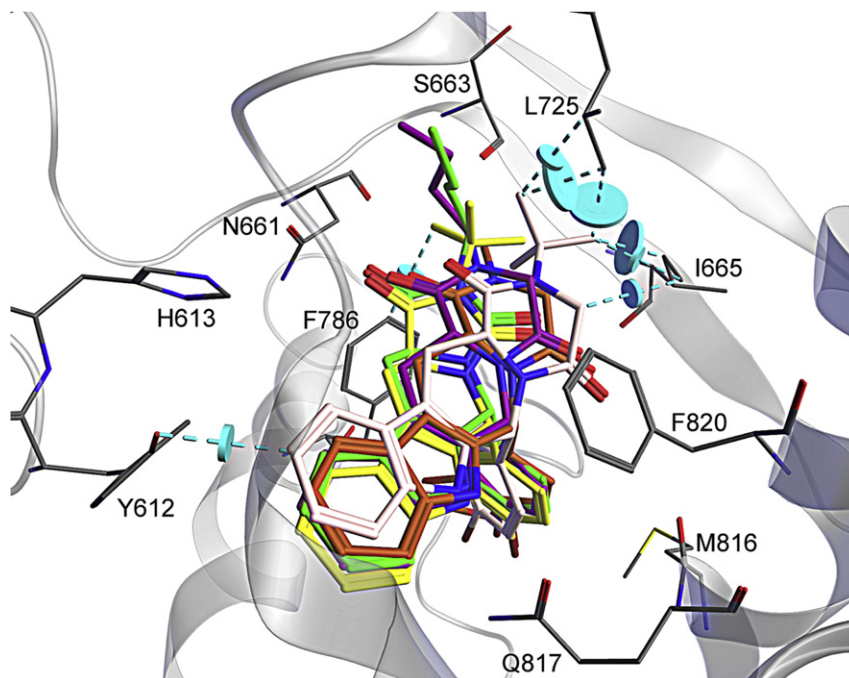


Fig. 4. Binding poses of compounds **12** (green), **20** (yellow), **33** (violet) and **37** (rosa) and crystallographic pose of **1** (brown). Steric clashes (energy contribution >1 kcal/mol) between the *t*-butyl-bearing compounds **20** and **37** and the amino acid residues Tyr612, Ile665, Leu725, and F786 are shown as cyan dots and discs, and might explain the reduced inhibitory potency. (For interpretation of the references to colour in this figure legend, the reader is referred to the web version of this article.)

silica gel plates (ALUGRAM SIL G/UV254) and detection of the components was made by short UV light. Column chromatography was performed using silica-gel (70–200 μm). Melting points were determined on Buchi Melting Point apparatus and are uncorrected. FTIR spectra were recorded on Nicolet Avatar 380 spectrometer. ^1H spectra were run at 300 MHz and ^{13}C spectra were run at 75.46 MHz

in deuterated chloroform (CDCl_3) and dimethylsulfoxide (DMSO). Chemical shifts (δ) were reported in parts per million (ppm) downfield from TMS; multiplicities are abbreviated as: s: singlet; d: doublet; t: triplet; q: quartet; m: multiplet; dd: doublet of doublet; brs: broad. Mass spectra were made on Focus GC/Polaris MS, model 5890; series II at an ionization potential of 70 eV. Elemental analysis

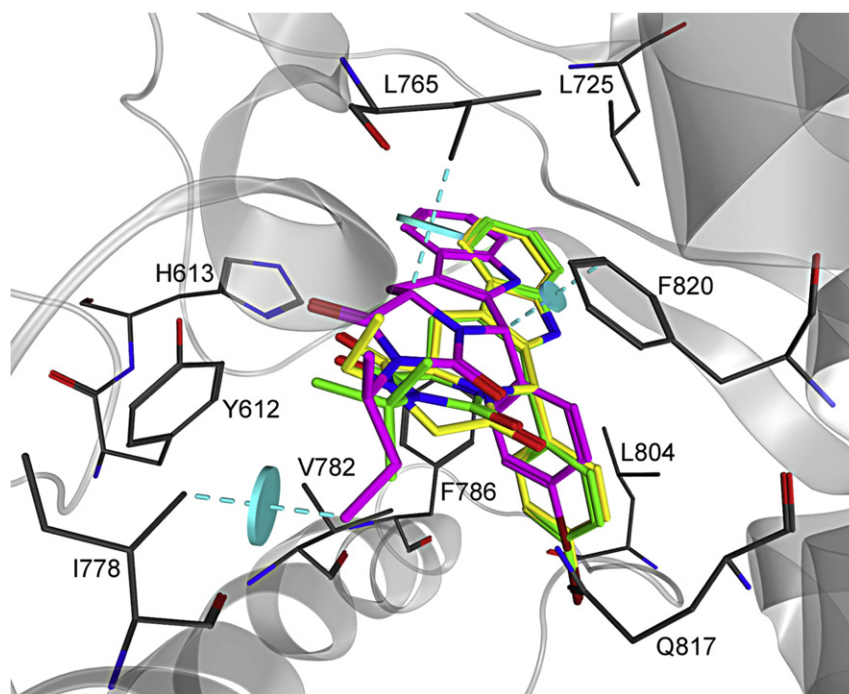


Fig. 5. Binding modes of the best ranked poses of the 5/6 *S*-isomer compounds **15** (magenta; clashes with Ile778, Leu765 as orange disks), **18** (green) and **30** (yellow). Steric clashes with Leu765, Ile778 and F820 are rendered as cyan dots and discs. (For interpretation of the references to colour in this figure legend, the reader is referred to the web version of this article.)

were performed by the Microanalytical Unit, Faculty of Science, Cairo University; the found values were within $\pm 0.4\%$ of the theoretical ones, unless otherwise indicated. D- & L-Tryptophan methyl ester were prepared by a known procedure [22–24].

5.2. Methods

5.2.1. General procedures for the preparation of methyl-1-(4-bromophenyl)-2,3,4,9-tetrahydro-1H- β -carboline-3-carboxylate (**1–4**)

The appropriate tryptophan methyl ester (11.8 g, 54.16 mmol) was added to 4-bromobenzaldehyde (11 g, 59.48 mmol) and dissolved in CH_2Cl_2 (10 mL). The solution was cooled to 0°C in an ice bath. To this solution TFA (3 mL) was added dropwise, and the mixture was stirred at room temperature for 4 days under N_2 atmosphere. The reaction mixture was then basified with dilute NH_4OH solution and extracted with CH_2Cl_2 (3×50 mL). The organic layer was washed with water, brine, dried over anhydrous Na_2SO_4 , filtered, and evaporated under reduced pressure. The residue was purified and the isomers were separated by column chromatography on silica gel eluting with CH_2Cl_2 , to give first the appropriate *cis*-isomer followed by the *trans*-one.

5.2.1.1. Methyl (1R,3R)-1-(4-bromophenyl)-2,3,4,9-tetrahydro-1H- β -carboline-3-carboxylate (1**).** Yield 34%; yellow powder; mp $202\text{--}205^\circ\text{C}$; $R_f = 0.72$ ($\text{CH}_2\text{Cl}_2/\text{MeOH}$ 99:1); IR (cm^{-1}): 3375 (–NH–), 1737 (–CO–). ^1H NMR: δ 10.3 (s, 1H, NH), 7.56–7.53 (m, 2H, Ar), 7.46–7.43 (d, 1H, Ar), 7.34–7.31 (m, 2H, Ar), 7.24–7.21 (m, 1H, Ar), 7.05–6.94 (m, 2H, Ar), 5.23 (s, 1H, CHPh), 3.91–3.86 (dd, $J = 10.93, 4.16$ Hz, 1H, CHCOOCH_3), 3.72 (s, 3H, OCH_3), 3.08–3.2 (m, 1H, CH_aH_b), 2.91–2.82 (m, 1H, CH_aH_b). ^{13}C NMR: δ 172.52, 141.31, 136.29, 134.66, 130.96, 130.66, 126.34, 120.70, 120.60, 118.27, 117.37, 110.99, 106.91, 57.12 (C1), 56.06 (C3), 51.50, 25.16. MS: m/z 386 ($\text{M}^+ + 2$), m/z 384 (M^+), m/z 218 (100%). Elemental analysis: calculated for ($\text{C}_{19}\text{H}_{17}\text{BrN}_2\text{O}_2$) C, H, N.

5.2.1.2. Methyl (1S,3R)-1-(4-bromophenyl)-2,3,4,9-tetrahydro-1H- β -carboline-3-carboxylate (2**).** Yield 36%; yellow powder; mp $177\text{--}180^\circ\text{C}$; $R_f = 0.43$ ($\text{CH}_2\text{Cl}_2/\text{MeOH}$ 99:1); IR (cm^{-1}): 3334 (–NH–), 1709 (–CO–). ^1H NMR: δ 10.61 (s, 1H, NH), 7.53–7.44 (dd, 3H, Ar), 7.24 (t, 3H, Ar), 7.06–6.97 (m, 2H, Ar), 5.32 (s, 1H, CHPh), 3.80–3.75 (dd, $J = 7.09, 5.39$ Hz, 1H, CHCOOCH_3), 3.63 (s, 3H, OCH_3), 3.10–3.04 (dd, $J = 15.17, 5.14$ Hz, 1H, CH_aH_b), 2.95–2.87 (dd, $J = 15.21, 7.32$ Hz, 1H, CH_aH_b). ^{13}C NMR: δ 173.47, 142.26, 136.05, 133.62, 130.80, 130.26, 126.35, 120.72, 120.14, 118.22, 118.43, 110.88, 106.56, 53.29 (C1), 51.71 (C3), 51.37, 24.52. MS: m/z 386 ($\text{M}^+ + 2$), m/z 384 (M^+), 100%. Elemental analysis: calculated for ($\text{C}_{19}\text{H}_{17}\text{BrN}_2\text{O}_2$) C, H, N.

5.2.1.3. Methyl (1S,3S)-1-(4-bromophenyl)-2,3,4,9-tetrahydro-1H- β -carboline-3-carboxylate (3**).** Yield 33%; yellow powder; mp $205\text{--}207^\circ\text{C}$; $R_f = 0.73$ ($\text{CH}_2\text{Cl}_2/\text{MeOH}$ 99:1); IR (cm^{-1}): 3382 (–NH–), 1726 (–CO–). ^1H NMR: δ 10.32 (s, 1H, NH), 7.54–7.42 (dd, 2H, Ar), 7.32–7.21 (m, 4H, Ar), 7.03–6.95 (m, 2H, Ar), 5.20 (s, 1H, CHPh), (dd, $J = 10.93, 4.16$ Hz, 1H, CHCOOCH_3), 3.70 (s, 3H, OCH_3), 3.08–3.04 (m, 1H, CH_aH_b), 2.90–2.82 (m, 1H, CH_aH_b). ^{13}C NMR: δ 172.63, 141.12, 136.45, 134.64, 131.21, 130.98, 126.45, 120.95, 120.91, 118.54, 117.65, 111.24, 107.03, 57.16 (C1), 56.15 (C3), 51.86, 25.21. MS: m/z 386 ($\text{M}^+ + 2$), m/z 384 (M^+), m/z 218 (100%). Elemental analysis: calculated for ($\text{C}_{19}\text{H}_{17}\text{BrN}_2\text{O}_2$) C, H, N.

5.2.1.4. Methyl (1R,3S)-1-(4-bromophenyl)-2,3,4,9-tetrahydro-1H- β -carboline-3-carboxylate (4**).** Yield 42%; yellow powder; mp $179\text{--}182^\circ\text{C}$; $R_f = 0.43$ ($\text{CH}_2\text{Cl}_2/\text{MeOH}$ 99:1); IR (cm^{-1}): 3333 (–NH–), 1709 (–CO–). ^1H NMR: δ 10.59 (s, 1H, NH), 7.53–7.45 (dd, 3H,

Ar), 7.29–7.23 (t, 3H, Ar), 7.08–6.96 (m, 2H, Ar), 5.35 (s, 1H, CHPh), 3.83–3.78 (t, 1H, CHCOOCH_3), 3.64 (s, 3H, OCH_3), 3.13–3.06 (dd, $J = 15.18, 5.12$ Hz, 1H, CH_aH_b), 2.97–2.90 (dd, $J = 15.18, 7.38$ Hz, 1H, CH_aH_b). ^{13}C NMR: δ 173.66, 142.39, 136.18, 133.76, 130.97, 130.45, 126.48, 120.90, 120.34, 118.40, 117.60, 111.05, 106.70, 53.44 (C1), 51.85 (C3), 51.57, 24.68. MS: m/z 386 ($\text{M}^+ + 2$), m/z 384 (M^+), 100%. Elemental analysis: calculated for ($\text{C}_{19}\text{H}_{17}\text{BrN}_2\text{O}_2$) C, H, N.

5.2.1.5. General procedures for the preparation of: 2-alkyl-5-(4-bromophenyl)-5,6,11,11a-tetrahydro-1H-imidazo [1',5':1,6]pyrido [3,4-b]indole-1,3(2H)-dione (5–20**).** Excess alkyl isocyanate (1.6 mmol) was added to a well stirred solution of the appropriate beta carboline **1–4** (0.38 g, 1 mmol) in methyl ethyl ketone (10 mL). The mixture was then stirred at reflux for 16 h under N_2 atmosphere. The solvent was evaporated under reduced pressure, the residue was purified using column chromatography on silica gel, eluting with CH_2Cl_2 .

5.2.1.6. (5R,11aR)-5-(4-Bromophenyl)-2-ethyl-5,6,11,11a-tetrahydro-1H-imidazo[1',5':1,6]pyrido[3,4-b]indole-1,3(2H)-dione (5**).** Yield 20%; yellowish white powder; mp $250\text{--}253^\circ\text{C}$; $R_f = 0.51$ ($\text{CH}_2\text{Cl}_2/\text{MeOH}$ 99.5:0.5); IR (cm^{-1}): 3240 (–NH–), 1703, 1692 (–CO–). ^1H NMR: δ 7.85 (s, 1H, NH), 7.66–7.63 (m, 1H, Ar), 7.57–7.54 (m, 1H, Ar), 7.25–7.06 (m, 6H, Ar), 6.49 (s, 1H, CHPh), 4.41–4.37 (m, 1H, CHC(O)N), 3.57–3.51 (m, 3H, $\text{NCH}_2 + \text{CH}_a\text{H}_b$), 3.10–3.01 (m, 1H, CH_aH_b), 1.23–1.18 (t, 3H, CH_3). MS: m/z 425 ($\text{M}^+ + 2$), m/z 423 (M^+), m/z 218 (100%). Elemental analysis: calculated for ($\text{C}_{21}\text{H}_{18}\text{BrN}_3\text{O}_2$) C, H, N.

5.2.1.7. (5S,11aR)-5-(4-Bromophenyl)-2-ethyl-5,6,11,11a-tetrahydro-1H-imidazo[1',5':1,6]pyrido[3,4-b]indole-1,3(2H)-dione (6**).** Yield 27%; yellow powder; mp $110\text{--}113^\circ\text{C}$; $R_f = 0.6$ ($\text{CH}_2\text{Cl}_2/\text{MeOH}$ 99.5:0.5); IR (cm^{-1}): 3311 (–NH–), 1763, 1691 (–CO–). ^1H NMR: δ 7.84 (s, 1H, NH), 7.59–7.56 (m, 1H, Ar), 7.51–7.48 (m, 1H, Ar), 7.33–7.16 (m, 6H, Ar), 6.30 (s, 1H, CHPh), 4.30–4.24 (dd, $J = 11.1, 5.1$ Hz, 1H, CHC(O)N), 3.66–3.58 (m, 2H, NCH_2), 3.54–3.47 (dd, $J = 15.45, 5.4$ Hz, 1H, CH_aH_b), 2.94–2.85 (ddd, $J = 15.38, 11.01$ Hz, 1H, CH_aH_b), 1.28–1.26 (t, 3H, CH_3). MS: m/z 425 ($\text{M}^+ + 2$), m/z 423 (M^+), m/z 218 (100%). Elemental analysis: calculated for ($\text{C}_{21}\text{H}_{18}\text{BrN}_3\text{O}_2$) C, H, N.

5.2.1.8. (5S,11aS)-5-(4-Bromophenyl)-2-ethyl-5,6,11,11a-tetrahydro-1H-imidazo[1',5':1,6]pyrido[3,4-b]indole-1,3(2H)-dione (7**).** Yield 23%; yellowish white powder; mp $251\text{--}253^\circ\text{C}$; $R_f = 0.51$ ($\text{CH}_2\text{Cl}_2/\text{MeOH}$ 99.5:0.5); IR (cm^{-1}): 3241 (–NH–), 1703, 1692 (–CO–). ^1H NMR: δ 7.86 (s, 1H, NH), 7.63–7.54 (m, 2H, Ar), 7.27–7.03 (m, 6H, Ar), 6.49 (s, 1H, CHPh), 4.41–4.37 (m, 1H, CHC(O)N), 3.56–3.49 (m, 3H, $\text{NCH}_2 + \text{CH}_a\text{H}_b$), 3.10–3.01 (m, 1H, CH_aH_b), 1.23–1.18 (t, 3H, CH_3). MS: m/z 425 ($\text{M}^+ + 2$), m/z 423 (M^+), m/z 218 (100%). Elemental analysis: calculated for ($\text{C}_{21}\text{H}_{18}\text{BrN}_3\text{O}_2$) C, H, N.

5.2.1.9. (5R,11aS)-5-(4-Bromophenyl)-2-ethyl-5,6,11,11a-tetrahydro-1H-imidazo[1',5':1,6]pyrido[3,4-b]indole-1,3(2H)-dione (8**).** Yield 25%; yellow powder; mp $115\text{--}118^\circ\text{C}$; $R_f = 0.6$ ($\text{CH}_2\text{Cl}_2/\text{MeOH}$ 99.5:0.5); IR (cm^{-1}): 3313 (–NH–), 1763, 1692 (–CO–). ^1H NMR: δ 7.76 (s, 1H, NH), 7.59–7.56 (d, 1H, Ar), 7.51–7.49 (m, 2H, Ar), 7.33–7.24 (m, 5H, Ar), 6.29 (s, 1H, CHPh), 4.30–4.24 (dd, $J = 11.00, 5.51$ Hz, 1H, CHC(O)N), 3.62–3.59 (m, 2H, NCH_2), 3.55–3.48 (dd, $J = 15.38, 5.55$ Hz, 1H, CH_aH_b), 2.95–2.85 (ddd, $J = 15.38, 11.00, 1.80$ Hz, 1H, CH_aH_b), 1.26–1.23 (t, 3H, CH_3). MS: m/z 425 ($\text{M}^+ + 2$), m/z 423 (M^+), m/z 218 (100%). Elemental analysis: calculated for ($\text{C}_{21}\text{H}_{18}\text{BrN}_3\text{O}_2$) C, H, N.

5.2.1.10. (5R,11aR)-5-(4-Bromophenyl)-2-butyl-5,6,11,11a-tetrahydro-1H-imidazo[1',5':1,6]pyrido[3,4-b]indole-1,3(2H)-dione (9**).** Yield 38%; yellowish white powder; mp $225\text{--}228^\circ\text{C}$; $R_f = 0.48$ ($\text{CH}_2\text{Cl}_2/\text{MeOH}$ 99.5:0.5); IR (cm^{-1}): 3298 (–NH–), 1766, 1692.3 (–CO–). ^1H

NMR: δ 7.89 (s, 1H, NH), 7.57–7.56 (d, 2H, Ar), 7.48–7.44 (d, 1H, Ar), 7.27–7.17 (m, 5H, Ar), 5.77 (s, 1H, CHPh), 4.42–4.30 (dd, $J = 11.4$, 4.5 Hz, 1H, CHC(O)N), 3.51–3.46 (m, 3H, NCH₂ + CH_aH_b), 3.11–2.94 (dd, 1H, CH_aH_b), 1.62–1.54 (m, 2H, CH₂CH₂CH₃), 1.33–1.27 (m, 2H, CH₂CH₃), 0.94–0.89 (t, 3H, CH₃). MS: m/z 453 ($M^+ + 2$), m/z 451 (M^+), m/z 218 (100%). Elemental analysis: calculated for (C₂₃H₂₂BrN₃O₂) C, H, N.

5.2.1.11. (5*S*,11*aR*)-5-(4-Bromophenyl)-2-butyl-5,6,11,11*a*-tetrahydro-1*H*-imidazo[1',5':1,6]pyrido[3,4-*b*]indole-1,3(2*H*)-dione (**10**). Yield 45%; yellow powder; mp 188–191 °C; $R_f = 0.7$ (CH₂Cl₂/MeOH 99.5:0.5); IR (cm⁻¹): 3303 (–NH–), 1760, 1692 (–CO–). ¹H NMR: δ 7.85 (s, 1H, NH), 7.58–7.56 (m, 1H, Ar), 7.50–7.48 (m, 1H, Ar), 7.32–7.19 (m, 6H, Ar), 6.28 (s, 1H, CHPh), 4.29–4.24 (dd, $J = 11.00$, 5.50 Hz, 1H, CHC(O)N), 3.55–3.48 (m, 3H, NCH₂ + CH_aH_b), 2.93–2.85 (m, 1H, CH_aH_b), 1.64–1.59 (m, 2H, CH₂CH₂CH₃), 1.27–1.24 (m, 2H, CH₂CH₃), 0.96–0.93 (t, 3H, CH₃). MS: m/z 453 ($M^+ + 2$), m/z 451 (M^+), m/z 218 (100%). Elemental analysis: calculated for (C₂₃H₂₂BrN₃O₂) C, H, N.

5.2.1.12. (5*S*,11*aS*)-5-(4-Bromophenyl)-2-butyl-5,6,11,11*a*-tetrahydro-1*H*-imidazo[1',5':1,6]pyrido[3,4-*b*]indole-1,3(2*H*)-dione (**11**). Yield 35%; yellowish white powder; mp 227–228 °C; $R_f = 0.48$ (CH₂Cl₂/MeOH 99.5:0.5); IR (cm⁻¹): 3294 (–NH–), 1766, 1692 (–CO–). ¹H NMR: δ 7.90 (s, 1H, NH), 7.59–7.56 (m, 2H, Ar), 7.48–7.46 (d, 1H, Ar), 7.23–7.16 (m, 5H, Ar), 5.78 (s, 1H, CHPh), 4.41–4.31 (dd, $J = 11.4$, 4.5 Hz, 1H, CHC(O)N), 3.55–3.44 (m, 3H, NCH₂ + CH_aH_b), 3.09–3.00 (m, 1H, CH_aH_b), 1.62–1.54 (m, 2H, CH₂CH₂CH₃), 1.33–1.27 (m, 2H, CH₂CH₃), 0.94–0.89 (t, 3H, CH₃). MS: m/z 453 ($M^+ + 2$), m/z 451 (M^+), m/z 218 (100%). Elemental analysis: calculated for (C₂₃H₂₂BrN₃O₂) C, H, N.

5.2.1.13. (5*R*,11*aS*)-5-(4-Bromophenyl)-2-butyl-5,6,11,11*a*-tetrahydro-1*H*-imidazo[1',5':1,6]pyrido[3,4-*b*]indole-1,3(2*H*)-dione (**12**). Yield 47%; yellow powder; mp 186–188 °C; $R_f = 0.7$ (CH₂Cl₂/MeOH 99.5:0.5); IR (cm⁻¹): 3315 (–NH–), 1763, 1692 (–CO–). ¹H NMR: δ 7.85 (s, 1H, NH), 7.58–7.47 (dd, 3H, Ar), 7.32–7.19 (m, 5H, Ar), 6.27 (s, 1H, CHPh), 4.29–4.24 (dd, $J = 11.00$, 5.50 Hz, 1H, CHC(O)N), 3.56–3.48 (m, 3H, NCH₂ + CH_aH_b), 3.94–3.84 (m, 1H, CH_aH_b), 1.64–1.59 (m, 2H, CH₂CH₂CH₃), 1.35–1.27 (m, 2H, CH₂CH₃), 0.96–0.91 (t, 3H, CH₃). MS: m/z 453 ($M^+ + 2$), m/z 451 (M^+), m/z 218 (100%). Elemental analysis: calculated for (C₂₃H₂₂BrN₃O₂) C, H, N.

5.2.1.14. (5*R*,11*aR*)-5-(4-Bromophenyl)-2-sec-butyl-5,6,11,11*a*-tetrahydro-1*H*-imidazo[1',5':1,6]pyrido[3,4-*b*]indole-1,3(2*H*)-dione (**13**). Yield 50%; yellow powder; mp 233–235 °C; $R_f = 0.27$ (CH₂Cl₂); IR (cm⁻¹): 3291 (–NH–), 1762, 1692 (–CO–). ¹H NMR: δ 7.89 (s, 1H, NH), 7.58–7.56 (d, 2H, Ar), 7.48–7.45 (d, 2H, Ar), 7.21–7.15 (m, 4H, Ar), 5.75 (s, 1H, CHPh), 4.35–4.30 (m, 1H, CHC(O)N), 4.05–4.00 (m, 1H, NCH), 3.54–3.48 (m, 1H, CH_aH_b), 3.08–2.98 (m, 1H, CH_aH_b), 2.01–1.88 (m, 1H, NCHCH_aH_b), 1.78–1.64 (m, 1H, NCHCH_aH_b), 1.40–1.37 (dd, 3H, CHCH₃), 0.88–0.83 (t, 3H, CH₂CH₃). MS: m/z 453 ($M^+ + 2$), m/z 451 (M^+), m/z 218 (100%). Elemental analysis: calculated for (C₂₃H₂₂BrN₃O₂) C, H, N.

5.2.1.15. (5*S*,11*aR*)-5-(4-Bromophenyl)-2-sec-butyl-5,6,11,11*a*-tetrahydro-1*H*-imidazo[1',5':1,6]pyrido[3,4-*b*]indole-1,3(2*H*)-dione (**14**). Yield 48%; yellow powder; mp 227–230 °C; $R_f = 0.45$ (CH₂Cl₂); IR (cm⁻¹): 3343 (–NH–), 1760, 1692 (–CO–). ¹H NMR: δ 7.81 (s, 1H, NH), 7.58–7.48 (dd, 3H, Ar), 7.32–7.21 (m, 5H, Ar), 6.26 (s, 1H, CHPh), 4.26–4.19 (m, 1H, CHC(O)N), 4.13–4.03 (m, 1H, NCH), 3.54–3.47 (dd, 1H, CH_aH_b), 2.92–2.83 (dd, 1H, CH_aH_b), 2.04–1.92 (m, 1H, NCHCH_aH_b), 1.79–1.67 (m, 1H, NCHCH_aH_b), 1.42–1.39 (d, 3H, CHCH₃), 0.89–0.84 (t, 3H, CH₂CH₃). MS: m/z 453 ($M^+ + 2$), m/z 451 (M^+), m/z 218 (100%). Elemental analysis: calculated for (C₂₃H₂₂BrN₃O₂) C, H, N.

5.2.1.16. (5*S*,11*aS*)-5-(4-Bromophenyl)-2-sec-butyl-5,6,11,11*a*-tetrahydro-1*H*-imidazo[1',5':1,6]pyrido[3,4-*b*]indole-1,3(2*H*)-dione (**15**). Yield 40%; yellow powder; mp 240–243 °C; $R_f = 0.5$ (CH₂Cl₂); IR (cm⁻¹): 3292 (–NH–), 1762, 1692 (–CO–). ¹H NMR: δ 7.85 (s, 1H, NH), 7.57–7.45 (m, 3H, Ar), 7.21–7.17 (m, 5H, Ar), 5.76 (s, 1H, CHPh), 4.36–4.30 (m, 1H, CHC(O)N), 4.07–3.98 (m, 1H, NCH), 3.54–3.47 (dd, 1H, CH_aH_b), 3.08–2.95 (m, 1H, CH_aH_b), 2.01–1.86 (m, 1H, NCHCH_aH_b), 1.76–1.62 (m, 1H, NCHCH_aH_b), 1.40–1.37 (dd, 3H, NCHCH₃), 0.88–0.83 (t, 3H, NCHCH₂CH₃). MS: m/z 453 ($M^+ + 2$), m/z 451 (M^+), m/z 218 (100%). Elemental analysis: calculated for (C₂₃H₂₂BrN₃O₂) C, H, N.

5.2.1.17. (5*R*,11*aS*)-5-(4-Bromophenyl)-2-sec-butyl-5,6,11,11*a*-tetrahydro-1*H*-imidazo[1',5':1,6]pyrido[3,4-*b*]indole-1,3(2*H*)-dione (**16**). Yield 34%; yellowish white powder; mp 230–233 °C; $R_f = 0.43$ (CH₂Cl₂); IR (cm⁻¹): 3342 (–NH–), 1759, 1692 (–CO–). ¹H NMR: δ 7.83 (s, 1H, NH), 7.58–7.56 (d, 1H, Ar), 7.51–7.47 (m, 2H, Ar), 7.32–7.18 (m, 5H, Ar), 6.26 (s, 1H, CHPh), 4.26–4.19 (m, 1H, CHC(O)N), 4.13–4.02 (m, 1H, NCH), 3.54–3.46 (dd, 1H, CH_aH_b), 2.92–2.83 (dd, 1H, CH_aH_b), 2.04–1.91 (m, 1H, NCHCH_aH_b), 1.79–1.67 (m, 1H, NCHCH_aH_b), 1.42–1.39 (d, 3H, NCHCH₃), 0.89–0.84 (t, 3H, NCHCH₂CH₃). MS: m/z 453 ($M^+ + 2$), m/z 451 (M^+), m/z 218 (100%). Elemental analysis: calculated for (C₂₃H₂₂BrN₃O₂) C, H, N.

5.2.1.18. (5*R*,11*aR*)-5-(4-Bromophenyl)-2-tert-butyl-5,6,11,11*a*-tetrahydro-1*H*-imidazo[1',5':1,6]pyrido[3,4-*b*]indole-1,3(2*H*)-dione (**17**). Yield 33%; yellowish white powder; mp 269–270 °C; $R_f = 0.29$ (CH₂Cl₂); IR (cm⁻¹): 3411 (–NH–), 1764, 1703 (–CO–). ¹H NMR: δ 7.8 (s, 1H, NH), 7.48–7.45 (d, 2H, Ar), 7.21–7.16 (m, 6H, Ar), 5.7 (s, 1H, CHPh), 4.24–4.20 (dd, 1H, CHC(O)N), 3.49–3.42 (dd, 1H, CH_aH_b), 3.05–2.94 (m, 1H, CH_aH_b), 1.59 (s, 9H, CH₃). MS: m/z 453 ($M^+ + 2$), m/z 451 (M^+), m/z 218 (100%). Elemental analysis: calculated for (C₂₃H₂₂BrN₃O₂) C, H, N.

5.2.1.19. (5*S*,11*aR*)-5-(4-Bromophenyl)-2-tert-butyl-5,6,11,11*a*-tetrahydro-1*H*-imidazo[1',5':1,6]pyrido[3,4-*b*]indole-1,3(2*H*)-dione (**18**). Yield 53%; yellow powder; mp 137–140 °C; $R_f = 0.49$ (CH₂Cl₂); IR (cm⁻¹): 3327 (–NH–), 1760, 1692 (–CO–). ¹H NMR: δ 7.74 (s, 1H, NH), 7.51–7.48 (m, 2H, Ar), 7.27–7.21 (m, 6H, Ar), 6.2 (s, 1H, CHPh), 4.17–4.12 (dd, 1H, CHC(O)N), 3.50–3.43 (dd, 1H, CH_aH_b), 2.90–2.81 (m, 1H, CH_aH_b), 1.62 (s, 9H, CH₃). MS: m/z 453 ($M^+ + 2$), m/z 451 (M^+), m/z 218 (100%). Elemental analysis: calculated for (C₂₃H₂₂BrN₃O₂) C, H, N.

5.2.1.20. (5*S*,11*aS*)-5-(4-Bromophenyl)-2-tert-butyl-5-(4-bromophenyl)-5,6,11,11*a*-tetrahydro-1*H*-imidazo[1',5':1,6]pyrido[3,4-*b*]indole-1,3(2*H*)-dione (**19**). Yield 50%; yellowish white powder; mp 265–268 °C; $R_f = 0.27$ (CH₂Cl₂); IR (cm⁻¹): 3295 (–NH–), 1762, 1692.4 (–CO–). ¹H NMR: δ 7.73 (s, 1H, NH), 7.50–7.45 (m, 2H, Ar), 7.21–7.17 (m, 6H, Ar), 5.71 (s, 1H, CHPh), 4.25–4.20 (dd, 1H, CHC(O)N), 3.49–3.42 (dd, 1H, CH_aH_b), 3.05–2.95 (m, 1H, CH_aH_b), 1.59 (s, 9H, CH₃). MS: m/z 453 ($M^+ + 2$), m/z 451 (M^+), m/z 218 (100%). Elemental analysis: calculated for (C₂₃H₂₂BrN₃O₂) C, H, N.

5.2.1.21. (5*R*,11*aS*)-5-(4-Bromophenyl)-2-tert-butyl-5,6,11,11*a*-tetrahydro-1*H*-imidazo[1',5':1,6]pyrido[3,4-*b*]indole-1,3(2*H*)-dione (**20**). Yield 42%; yellow powder; mp 139–142 °C; $R_f = 0.48$ (CH₂Cl₂); IR (cm⁻¹): 3326 (–NH–), 1761, 1691 (–CO–). ¹H NMR: δ 7.74 (s, 1H, NH), 7.51–7.49 (m, 2H, Ar), 7.27–7.20 (m, 6H, Ar), 6.23 (s, 1H, CHPh), 4.17–4.10 (m, 1H, CHC(O)N), 3.50–3.42 (dd, 1H, CH_aH_b), 2.90–2.80 (m, 1H, CH_aH_b), 1.63 (s, 9H, CH₃). MS: m/z 453 ($M^+ + 2$), m/z 451 (M^+), m/z 218 (100%). Elemental analysis: calculated for (C₂₃H₂₂BrN₃O₂) C, H, N.

5.2.1.22. General procedures for the preparation of methyl-1-(4-bromophenyl)-2-(2-chloroacetyl)-2,3,4,9-tetrahydro-1H- β -carboline-3-carboxylate (21–24**).** Chloroacetyl chloride (0.74 mL, 9.34 mmol) was added dropwise to a well stirred solution of the appropriate β -carboline (**1–4**) **1** (1.5 g, 3.89 mmol) and NaHCO₃ (0.39 g, 4.7 mmol) in CHCl₃ (40 mL) under ice cooling. The mixture was then stirred at room temperature under a nitrogen atmosphere for 1 h. The mixture was diluted with CH₂Cl₂, washed with a solution of NaHCO₃, brine, dried over Na₂SO₄, and evaporated under reduced pressure. The residue was then crystallized from diethyl ether.

5.2.1.23. Methyl (1R,3R)-1-(4-bromophenyl)-2-(chloroacetyl)-2,3,4,9-tetrahydro-1H- β -carboline-3-carboxylate (21**).** Yield 85%; yellow powder; mp 237–240 °C; $R_f = 0.41$ (CH₂Cl₂); IR (cm⁻¹): 3244 (–NH–), 1729, 1657 (–CO–). ¹H NMR: δ 8.00 (brs, 1H, NH), 7.88–7.85 (d, 1H, Ar), 7.57–7.54 (d, 1H, Ar), 7.31–7.14 (m, 6H, Ar), 6.73 (s, 1H, CHPh), 5.18–5.14 (m, 1H, CHCOOCH₃), 4.19–4.15 (m, 2H, COCH₂Cl), 3.64 (s, 3H, OCH₃), 3.37–3.33 (dd, 1H, CH_aCH_b), 3.14–3.06 (dd, 1H, CH_aH_b). MS: m/z 464 (M⁺ + 4), m/z 462 (M⁺ + 2), m/z 460 (M⁺), m/z 383 (100%). Elemental analysis: calculated for (C₂₁H₁₈BrClN₂O₃) C, H, N.

5.2.1.24. Methyl (1S,3R)-1-(4-chlorophenyl)-2-(chloroacetyl)-2,3,4,9-tetrahydro-1H- β -carboline-3-carboxylate (22**).** Yield 90%; yellowish green powder; mp 110–113 °C; $R_f = 0.17$ (CH₂Cl₂); IR (cm⁻¹): 3323 (–NH–), 1736, 1658 (–CO–). ¹H NMR: δ 2.2 (s, 1H, NH), 7.61–7.50 (m, 2H, Ar), 7.28–7.08 (m, 6H, Ar), 6.65 (s, 1H, CHPh), 5.31–5.28 (m, 1H, CHCOOCH₃), 4.19–4.06 (m, 2H, COCH₂Cl), 3.82 (s, 3H, OCH₃), 3.38–3.29 (dd, 1H, CH_aH_b), 3.14–3.07 (dd, 1H, CH_aH_b). MS: m/z 464 (M⁺ + 4), m/z 462 (M⁺ + 2), m/z 460 (M⁺), m/z 385 (100%). Elemental analysis: calculated for (C₂₁H₁₈BrClN₂O₃) C, H, N.

5.2.1.25. Methyl (1S,3S)-1-(4-bromophenyl)-2-(2-chloroacetyl)-2,3,4,9-tetrahydro-1H- β -carboline-3-carboxylate (23**).** Yield 82%; yellowish green powder; mp 227–230 °C; $R_f = 0.41$ (CH₂Cl₂); IR (cm⁻¹): 3345 (–NH–), 1730, 1657 (–CO–). ¹H NMR: δ 7.97 (brs, 1H, NH), 7.68–7.65 (d, 1H, Ar), 7.57–7.54 (d, 1H, Ar), 7.31–7.12 (m, 6H, Ar), 6.73 (s, 1H, CHPh), 5.18–5.14 (m, 1H, CHCOOCH₃), 4.19–4.15 (m, 2H, COCH₂Cl), 3.64 (brs, 3H, OCH₃), 3.37–3.33 (dd, 1H, CH_aH_b), 3.14–3.07 (dd, 1H, CH_aH_b). MS: m/z 464 (M⁺ + 4), m/z 462 (M⁺ + 2), m/z 460 (M⁺), m/z 383 (100%). Elemental analysis: calculated for (C₂₁H₁₈BrClN₂O₃) C, H, N.

5.2.1.26. Methyl (1R,3S)-1-(4-chlorophenyl)-2-(chloroacetyl)-2,3,4,9-tetrahydro-1H- β -carboline-3-carboxylate (24**).** Yield 93%; yellowish green powder; mp 110–114 °C; $R_f = 0.17$ (CH₂Cl₂); IR (cm⁻¹): 3324 (–NH–), 1727, 1658 (–CO–). ¹H NMR: δ 8.22 (s, 1H, NH), 7.62–7.50 (m, 2H, Ar), 7.29–7.08 (m, 6H, Ar), 6.65 (s, 1H, CHPh), 5.31–5.27 (m, 1H, CHCOOCH₃), 4.19–4.06 (m, 2H, COCH₂Cl), 3.64 (s, 1H, OCH₃), 3.35–3.32 (dd, 1H, CH_aH_b), 3.15–3.07 (dd, 1H, CH_aH_b). MS: m/z 464 (M⁺ + 4), m/z 462 (M⁺ + 2), m/z 460 (M⁺), m/z 385 (100%). Elemental analysis: calculated for (C₂₁H₁₈BrClN₂O₃) C, H, N.

5.2.1.27. General procedures for the preparation of 2-alkyl-6-(4-bromophenyl)-2,3,6,7,12,12a-hexahydropyrazino [1',2':1,6]pyrido[3,4-b]indole-1,4-dione (25–40**).** A solution of the appropriate chloroacetyl derivative (**21–24**) (1.4 mmol, 1 equiv, 0.646 g) and the appropriate alkylamine (2.8 mmol, 2 equiv) in methanol (25 mL) was refluxed under a nitrogen atmosphere for 16 h. The reaction mixture was cooled to room temperature and evaporated to dryness under reduced pressure. The residue was dissolved in CH₂Cl₂, and the organic layer was washed with water, dried over Na₂SO₄, filtered, and concentrated to dryness. The crude product was then purified using column chromatography.

5.2.1.28. (6R,12aR)-6-(4-Bromophenyl)-2-methyl-2,3,6,7,12,12a-hexahydropyrazino [1',2':1,6]pyrido[3,4-b]indole-1,4-dione (25**).** Yield 37%; yellowish white powder; mp 266–269 °C; $R_f = 0.55$ (CH₂Cl₂/MeOH 97:3); IR (cm⁻¹): 3248 (–NH–), 1677, 1642 (–CO–). ¹H NMR: δ 7.92 (s, 1H, NH), 7.63–7.60 (m, 1H, Ar), 7.38–7.36 (d, 2H, Ar), 7.28–7.25 (m, 1H, Ar), 7.22–7.16 (m, 4H, Ar), 6.17 (s, 1H, CHPh), 4.35–4.29 (dd, 1H, CHC(O)N), 4.14–4.08 (d, 1H, CH_aH_bC(O)N), 3.96–3.90 (d, 1H, CH_aH_bC(O)N), 3.84–3.78 (dd, 1H, CH_aH_b), 3.26–3.17 (dd, 1H, CH_aH_b), 3.05 (s, 3H, NCH₃). MS: m/z 425 (M⁺ + 2), m/z 423 (M⁺), m/z 218 (100%). Elemental analysis: calculated for (C₂₁H₁₈BrN₃O₂) C, H, N.

5.2.1.29. (6S,12aR)-6-(4-Bromophenyl)-2-methyl-2,3,6,7,12,12a-hexahydropyrazino [1',2':1,6]pyrido[3,4-b]indole-1,4-dione (26**).** Yield 25%; white powder; mp 287–290 °C; $R_f = 0.52$ (CH₂Cl₂/MeOH 97:3); IR (cm⁻¹): 3271 (–NH–), 1657, 1641 (–CO–). ¹H NMR: δ 8.03 (s, 1H, NH), 7.56–7.53 (d, 1H, Ar), 7.44–7.41 (m, 2H, Ar), 7.33–7.14 (m, 5H, Ar), 6.90 (s, 1H, CHPh), 4.30–4.25 (dd, 1H, CHC(O)N), 4.17–4.11 (d, 1H, CH_aH_bC(O)N), 4.02–3.90 (d, 1H, CH_aH_bC(O)N), 3.60–3.54 (dd, 1H, CH_aH_b), 3.01–2.92 (m, 4H, CH_aH_b + NCH₃). MS: m/z 425 (M⁺ + 2), m/z 423 (M⁺), m/z 218 (100%). Elemental analysis: calculated for (C₂₁H₁₈BrN₃O₂) C, H, N.

5.2.1.30. (6S,12aS)-6-(4-Bromophenyl)-2-methyl-2,3,6,7,12,12a-hexahydropyrazino [1',2':1,6]pyrido[3,4-b]indole-1,4-dione (27**).** Yield 31%; yellow powder; mp 264–266 °C; $R_f = 0.52$ (CH₂Cl₂/MeOH 97:3); IR (cm⁻¹): 3234 (–NH–), 1677, 1642 (–CO–). ¹H NMR: δ 7.92 (s, 1H, NH), 7.39–7.36 (m, 2H, Ar), 7.28–7.16 (m, 6H, Ar), 6.17 (s, 1H, CHPh), 4.35–4.28 (dd, 1H, CHC(O)N), 4.14–4.08 (d, 1H, CH_aH_bC(O)N), 3.96–3.90 (d, 1H, CH_aH_bC(O)N), 3.84–3.78 (dd, 1H, CH_aH_b), 3.26–3.17 (dd, 1H, CH_aH_b), 3.05 (s, 3H, NCH₃). MS: m/z 425 (M⁺ + 2), m/z 423 (M⁺), m/z 218 (100%). Elemental analysis: calculated for (C₂₁H₁₈BrN₃O₂) C, H, N.

5.2.1.31. (6R,12aS)-6-(4-Bromophenyl)-2-methyl-2,3,6,7,12,12a-hexahydropyrazino [1',2':1,6]pyrido[3,4-b]indole-1,4-dione (28**).** Yield 20%; yellow powder; mp 190–194 °C; $R_f = 0.5$ (CH₂Cl₂/MeOH 97:3); IR (cm⁻¹): 3303 (–NH–), 1658, 1649 (–CO–). ¹H NMR: δ 7.82 (s, 1H, NH), 7.55–7.52 (m, 1H, Ar), 7.39–7.37 (d, 3H, Ar), 7.22–7.18 (m, 4H, Ar), 6.18 (s, 1H, CHPhAr), 4.34–4.30 (dd, 1H, CHC(O)N), 4.14–4.08 (d, 1H, CH_aH_bC(O)N), 3.96–3.90 (d, 1H, CH_aH_bC(O)N), 3.84–3.78 (dd, 1H, CH_aH_b), 3.26–3.17 (m, 1H, CH_aH_b), 3.05 (s, 3H, NCH₃). MS: m/z 425 (M⁺ + 2), m/z 423 (M⁺), m/z 218 (100%). Elemental analysis: calculated for (C₂₁H₁₈BrN₃O₂) C, H, N.

5.2.1.32. (6R,12aR)-2-Ethyl-6-(4-bromophenyl)-2,3,6,7,12,12a-hexahydropyrazino [1',2':1,6]pyrido[3,4-b]indole-1,4-dione (29**).** Yield 39%; yellow powder; mp 276–279 °C; $R_f = 0.63$ (CH₂Cl₂/MeOH 97:3); IR (cm⁻¹): 3185 (–NH–), 1657, 1650 (–CO–). ¹H NMR: δ 7.92 (s, 1H, NH), 7.62–7.60 (m, 1H, Ar), 7.39–7.36 (d, 2H, Ar), 7.29–7.24 (m, 1H, Ar), 7.21–7.17 (m, 4H, Ar), 6.19 (s, 1H, CHPh), 4.33–4.28 (dd, $J = 11.25, 4.44$ Hz, 1H, CHC(O)N), 4.13–4.07 (d, $J = 17.51$ Hz, 1H, CH_aH_bC(O)N), 3.95–3.89 (d, $J = 17.45$ Hz, 1H, CH_aH_bC(O)N), 3.83–3.76 (dd, $J = 16.11, 4.50$ Hz, 1H, CH_aH_b), 3.72–3.65 (m, 1H, NCH_bH_a), 3.42–3.35 (m, 1H, NCH_bH_a), 3.26–3.17 (dd, $J = 16.09, 11.47$ Hz, 1H, CH_aH_b), 1.23–1.18 (t, 3H, CH₃). MS: m/z 439 (M⁺ + 2), m/z 437 (M⁺), m/z 218 (100%). Elemental analysis: calculated for (C₂₂H₂₀BrN₃O₂) C, H, N.

5.2.1.33. (6S,12aR)-2-Ethyl-6-(4-bromophenyl)-2,3,6,7,12,12a-hexahydropyrazino [1',2':1,6]pyrido[3,4-b]indole-1,4-dione (30**).** Yield 30%; yellowish white powder; mp 260–263 °C; $R_f = 0.62$ (CH₂Cl₂/MeOH 97:3); IR (cm⁻¹): 3270 (–NH–), 1658, 1649 (–CO–).

¹H NMR: δ 7.84 (s, 1H, NH), 7.64–7.60 (m, 1H, Ar), 7.39–7.37 (d, 2H, Ar), 7.21–7.18 (m, 5H, Ar), 6.19 (s, 1H, CHPh), 4.34–4.29 (dd, $J = 10.65, 4.2$ Hz, 1H, CHC(O)N), 4.13–4.07 (d, $J = 17.7$ Hz, 1H, CH_aH_bC(O)N), 3.95–3.89 (d, $J = 17.4$ Hz, 1H, CH_aH_bC(O)N), 3.83–3.76 (dd, $J = 16.20, 4.50$ Hz, 1H, CH_aH_b), 3.72–3.65 (m, 1H, NCH_aH_b), 3.42–3.35 (m, 1H, NCH_aH_b), 3.26–3.17 (dd, $J = 16.45, 11.7$ Hz, 1H, CH_aH_b), 1.23–1.19 (t, 3H, CH₃). MS: m/z 439 (M⁺ + 2), m/z 437 (M⁺), m/z 217 (100%). Elemental analysis: calculated for (C₂₂H₂₀BrN₃O₂) C, H, N.

5.2.1.34. (6S,12aS)-2-Ethyl-6-(4-bromophenyl)-2,3,6,7,12,12a-hexahydropyrazino [1',2':1,6]pyrido[3,4-b]indole-1,4-dione (**31**). Yield 20%; yellow powder; mp 270–273 °C; $R_f = 0.62$ (CH₂Cl₂/MeOH 97:3); IR (cm⁻¹): 3187 (–NH–), 1658, 1651 (–CO–). ¹H NMR: δ 7.97 (s, 1H, NH), 7.61–7.60 (m, 1H, Ar), 7.39–7.36 (d, 2H, Ar), 7.29–7.24 (m, 1H, Ar), 7.21–7.17 (m, 4H, Ar), 6.20 (s, 1H, CHPh), 4.35–4.30 (dd, $J = 11.32, 4.10$ Hz, 1H, CHC(O)N), 4.14–4.08 (d, $J = 17.51$ Hz, 1H, CH_aH_bC(O)N), 3.95–3.89 (d, $J = 17.45$ Hz, 1H, CH_aH_bC(O)N), 3.83–3.76 (dd, $J = 16.11, 4.0$ Hz, 1H, CH_aH_b), 3.71–3.64 (m, 1H, NCH_aH_b), 3.43–3.35 (m, 1H, NCH_aH_b), 3.26–3.17 (dd, $J = 16.09, 11.47$ Hz, 1H, CH_aH_b), 1.22–1.18 (t, 3H, CH₃). MS: m/z 439 (M⁺ + 2), m/z 437 (M⁺), m/z 217 (100%). Elemental analysis: calculated for (C₂₂H₂₀BrN₃O₂) C, H, N.

5.2.1.35. (6R,12aS)-2-Ethyl-6-(4-bromophenyl)-2,3,6,7,12,12a-hexahydropyrazino [1',2':1,6]pyrido[3,4-b]indole-1,4-dione (**32**). Yield 23%; yellow powder; mp 265–268 °C; $R_f = 0.63$ (CH₂Cl₂/MeOH 97:3); IR (cm⁻¹): 3282 (–NH–), 1658, 1649 (–CO–). ¹H NMR: δ 7.87 (s, 1H, NH), 7.66–7.61 (m, 1H, Ar), 7.39–7.36 (d, 2H, Ar), 7.21–7.17 (m, 5H, Ar), 6.19 (s, 1H, CHPh), 4.34–4.29 (dd, 1H, CHC(O)N), 4.13–3.08 (d, $J = 17.48$ Hz, 1H, CH_aH_bC(O)N), 3.95–3.89 (d, $J = 17.45$ Hz, 1H, CH_aH_bC(O)N), 3.83–3.76 (dd, 1H, CH_aH_b), 3.73–3.66 (m, 1H, NCH_aH_b), 3.44–3.33 (m, 1H, NCH_aH_b), 3.26–3.17 (dd, 1H, CH_aH_b), 1.23–1.18 (t, 3H, CH₃). MS: m/z 439 (M⁺ + 2), m/z 437 (M⁺), m/z 218 (100%). Elemental analysis: calculated for (C₂₂H₂₀BrN₃O₂) C, H, N.

5.2.1.36. (6R,12aR)-2-Butyl-6-(4-bromophenyl)-2,3,6,7,12,12a-hexahydropyrazino[1',2':1,6]pyrido[3,4-b]indole-1,4-dione (**33**). Yield 30%, yellow brown powder; mp 130–133 °C; $R_f = 0.76$ (CH₂Cl₂/MeOH 97:3); IR (cm⁻¹): 3273 (–NH–), 1658, 1650 (–CO–). ¹H NMR: δ 7.96 (s, 1H, NH), 7.62–7.60 (m, 1H, Ar), 7.38–7.35 (d, 2H, Ar), 7.29–7.26 (m, 1H, Ar), 7.22–7.16 (m, 4H, Ar), 6.20 (s, 1H, CHPh), 4.33–4.28 (dd, $J = 11.40, 4.18$ Hz, 1H, CHC(O)N), 4.12–4.06 (d, $J = 17.38$ Hz, 1H, CH_aH_bC(O)N), 3.94–3.88 (d, $J = 17.50$ Hz, 1H, CH_aH_bC(O)N), 3.81–3.74 (dd, $J = 16.12, 4.57$ Hz, 1H, CH_aH_b), 3.62–3.33 (m, 1H, NCH_aH_b), 3.62–3.55 (m, 1H, NCH_aH_b), 3.40–3.30 (dd, $J = 16.05, 11.5$ Hz, 1H, CH_aH_b), 1.62–1.52 (m, 2H, CH₂CH₂CH₃), 1.39–1.31 (m, 2H, CH₂CH₃), 0.98–0.93 (t, 3H, CH₃). MS: m/z 467 (M⁺ + 2), m/z 465 (M⁺), m/z 218 (100%). Elemental analysis: calculated for (C₂₄H₂₄BrN₃O₂) C, H, N.

5.2.1.37. (6S,12aR)-2-Butyl-6-(4-bromophenyl)-2,3,6,7,12,12a-hexahydropyrazino [1',2':1,6]pyrido[3,4-b]indole-1,4-dione (**34**). Yield 25%, yellowish white powder; mp 207–210 °C; $R_f = 0.76$ (CH₂Cl₂/MeOH 97:3); IR (cm⁻¹): 3273 (–NH–), 1658, 1649.7 (–CO–). ¹H NMR: δ 7.88 (s, 1H, NH), 7.63–7.60 (d, 1H, Ar), 7.39–7.36 (m, 2H, Ar) 7.20–7.17 (m, 5H, Ar), 6.20 (s, 1H, CHPh), 4.35–4.26 (dd, $J = 11.7, 4.2$ Hz, 1H, CHC(O)N), 4.13–4.07 (d, $J = 17.7$ Hz, 1H, CH_aH_bC(O)N), 3.94–3.89 (d, $J = 17.4$ Hz, 1H, CH_aH_bC(O)N), 3.81–3.74 (dd, $J = 15.9, 4.5$ Hz, 1H, CH_aH_b), 3.59–3.53 (m, 1H, NCH_aH_b), 3.43–3.41 (m, 1H, NCH_aH_b), 3.26–3.17 (dd, $J = 15.6, 11.7$ Hz, 1H, CH_aH_b), 1.60–1.50 (m, 2H, CH₂CH₂CH₃), 1.36–1.29 (m, 2H, CH₂CH₃), 0.93–0.83 (t, 3H, CH₃). MS: m/z 467 (M⁺ + 2), m/z 465 (M⁺), m/z 218 (100%). Elemental analysis: calculated for (C₂₄H₂₄BrN₃O₂) C, H, N.

5.2.1.38. (6S,12aS)-2-Butyl-6-(4-bromophenyl)-2,3,6,7,12,12a-hexahydropyrazino[1',2':1,6]pyrido[3,4-b]indole-1,4-dione (**35**). Yield 28%, yellowish brown powder; mp 135–130 °C; $R_f = 0.77$ (CH₂Cl₂/MeOH 97:3); IR (cm⁻¹): 3278 (–NH–), 1658, 1650 (–CO–). ¹H NMR: δ 7.85 (s, 1H, NH), 7.63–7.60 (d, 1H, Ar), 7.39–7.37 (d, 2H, Ar), 7.21–7.16 (m, 5H, Ar), 6.20 (s, 1H, CHPh), 4.34–4.29 (dd, $J = 10.8, 4.5$ Hz, 1H, CHC(O)N), 4.12–4.07 (d, $J = 17.4$ Hz, 1H, CH_aH_bC(O)N), 3.95–3.89 (d, $J = 17.4$ Hz, 1H, CH_aH_bC(O)N), 3.81–3.74 (dd, $J = 16.2, 4.5$ Hz, 1H, CH_aH_b), 3.62–3.55 (m, 1H, NCH_aH_b), 3.40–3.30 (m, 1H, NCH_aH_b), 3.27–3.17 (dd, $J = 16.2, 11.4$ Hz, 1H, CH_aH_b), 1.57–1.54 (m, 2H, CH₂CH₂CH₃), 1.36–1.31 (m, 2H, CH₂CH₃), 0.98–0.93 (t, 3H, CH₃). MS: m/z 467 (M⁺ + 2), m/z 465 (M⁺), m/z 218 (100%). Elemental analysis: calculated for (C₂₄H₂₄BrN₃O₂) C, H, N.

5.2.1.39. (6R,12aS)-2-Butyl-6-(4-bromophenyl)-2,3,6,7,12,12a-hexahydropyrazino [1',2':1,6]pyrido[3,4-b]indole-1,4-dione (**36**). Yield 20%, whitish yellow powder; mp 203–206 °C; $R_f = 0.77$ (CH₂Cl₂/MeOH 97:3); IR (cm⁻¹): 3257 (–NH–), 1657, 1650 (–CO–). ¹H NMR: δ 7.83 (s, 1H, NH), 7.63–7.53 (m, 1H, Ar), 7.40–7.37 (m, 1H, Ar), 7.26–7.16 (m, 6H, Ar), 6.19 (s, 1H, CHPh), 4.35–4.26 (dd, $J = 11.7, 4.5$ Hz, 1H, CHC(O)N), 4.13–4.08 (d, $J = 17.4$ Hz, 1H, CH_aH_bC(O)N), 3.95–3.89 (d, $J = 17.4$ Hz, 1H, CH_aH_bC(O)N), 3.82–3.76 (dd, $J = 15.9, 4.5$ Hz, 1H, CH_aH_b), 3.72–3.63 (m, 1H, NCH_aH_b), 3.44–3.32 (m, 1H, NCH_aH_b), 3.26–3.17 (dd, $J = 15.6, 11.7$ Hz, 1H, CH_aH_b), 1.62–1.53 (m, 2H, CH₂CH₂CH₃), 1.37–1.27 (m, 2H, CH₂CH₃), 0.98–0.93 (t, 3H, CH₃). MS: m/z 467 (M⁺ + 2), m/z 465 (M⁺), m/z 218 (100%). Elemental analysis: calculated for (C₂₄H₂₄BrN₃O₂) C, H, N.

5.2.1.40. (6R,12aR)-6-(4-Bromophenyl)-2-tert-butyl-2,3,6,7,12,12a-hexahydropyrazino [1',2':1,6]pyrido[3,4-b]indole-1,4-dione (**37**). Yield 30%, yellowish white powder; mp 117–120 °C; $R_f = 0.72$ (CH₂Cl₂/MeOH 90:10); IR (cm⁻¹): 3278 (–NH–), 1730, 1657 (–CO–). ¹H NMR: δ 8.14 (s, 1H, NH), 7.56–7.54 (d, 2H, Ar), 7.34–7.33 (d, 2H, Ar), 7.20–7.12 (m, 4H, Ar), 6.91 (s, 1H, CHPh), 4.92–4.90 (dd, 1H, CHC(O)N), 4.73–4.71 (d, 1H, CH_aH_bC(O)N), 3.69–3.58 (m, 2H, CH_aH_bC(O)N + CH_aH_b), 2.94–2.89 (dd, 1H, CH_aH_b), 1.14 (s, 9H, CH₃). MS: m/z 467 (M⁺ + 2), m/z 465 (M⁺), m/z 218 (100%). Elemental analysis: calculated for (C₂₄H₂₄BrN₃O₂) C, H, N.

5.2.1.41. (6S,12aR)-6-(4-Bromophenyl)-2-tert-butyl-2,3,6,7,12,12a-hexahydropyrazino [1',2':1,6]pyrido[3,4-b]indole-1,4-dione (**38**). Yield 28%, yellowish white powder; mp 133–136 °C; $R_f = 0.73$ (CH₂Cl₂/MeOH 90:10); IR (cm⁻¹): 3170 (–NH–), 1728, 1665 (–CO–). ¹H NMR: δ 8.5 (s, 1H, NH), 7.50–7.45 (d, 2H, Ar), 7.36–7.25 (m, 4H, Ar), 7.15–7.08 (m, 2H, Ar), 6.44 (s, 1H, CHPh), 4.94–4.92 (m, 1H, CHC(O)N), 4.63–4.61 (d, 1H, CH_aH_bC(O)N), 4.12–4.07 (d, 1H, CH_aH_bC(O)N), 3.83–3.63 (m, 1H, CH_aH_b), 3.14–2.90 (m, 1H, CH_aH_b), 1.24 (s, 9H, CH₃). MS: m/z 467 (M⁺ + 2), m/z 465 (M⁺), m/z 218 (100%). Elemental analysis: calculated for (C₂₄H₂₄BrN₃O₂) C, H, N.

5.2.1.42. (6S,12aS)-6-(4-Bromophenyl)-2-tert-butyl-2,3,6,7,12,12a-hexahydropyrazino[1',2':1,6]pyrido[3,4-b]indole-1,4-dione (**39**). Yield 34%, yellowish white powder; mp 120–123 °C; $R_f = 0.72$ (CH₂Cl₂/MeOH 90:10); IR (cm⁻¹): 3291 (–NH–), 1730, 1657 (–CO–). ¹H NMR: δ 8.1 (s, 1H, NH), 7.57–7.56 (d, 2H, Ar), 7.35–7.33 (d, 2H, Ar), 7.21–7.11 (m, 4H, Ar), 6.92 (s, 1H, CHPh), 4.95–4.94 (m, 1H, CHC(O)N), 4.25–4.19 (d, 1H, CH_aH_bC(O)N), 3.67–3.58 (m, 2H, CH_aH_bC(O)N + CH_aH_b), 2.99–2.94 (m, 1H, CH_aH_b), 1.14 (s, 9H, CH₃). MS: m/z 467 (M⁺ + 2), m/z 465 (M⁺), m/z 218 (100%). Elemental analysis: calculated for (C₂₄H₂₄BrN₃O₂) C, H, N.

5.2.1.43. (6R,12aS)-6-(4-Bromophenyl)-2-tert-butyl-2,3,6,7,12,12a-hexahydropyrazino[1',2':1,6]pyrido[3,4-b]indole-1,4-dione (**40**). Yield 20%, yellowish white powder; mp 135–138 °C; $R_f = 0.73$

(CH₂Cl₂/MeOH 90:10); IR (cm⁻¹): 3255 (–NH–), 1729, 1658 (–CO–). ¹H NMR: δ 8.54 (s, 1H, NH), 7.79–7.75 (d, 2H, Ar), 7.55–7.53 (d, 2H, Ar), 7.34–7.14 (m, 4H, Ar), 6.81 (s, 1H, CHPh), 4.92–4.86 (dd, 1H, CHC(O)N), 4.12–4.02 (d, 1H, CH_aH_bC(O)N), 3.82–3.76 (d, 1H, CH_aH_bC(O)N), 3.65–3.59 (dd, 1H, CH₃H_b), 3.10–3.08 (dd, 1H, CH_aH_b), 1.27 (s, 9H, CH₃). MS: *m/z* 467 (M⁺ + 2), *m/z* 465 (M⁺), *m/z* 218 (100%). Elemental analysis: calculated for (C₂₄H₂₄BrN₃O₂) C, H, N.

5.3. Biological evaluation

All the synthesized compounds were evaluated for their inhibitory properties versus recombinant PDE5. Compounds showing PDE5 for compounds showing a cGMP percentage of inhibition >65%, their *in vitro* ability to inhibit the growth of breast cancer cell line MDA-MB-231 were determined. For all assays, tadalafil (PDE5/PDE11 inhibitor) was used for comparison. Compound **25**, was further tested against PDE3A cAMP, PDE3B cGMP, PDE4B, PDE11A cAMP, PDE11A cGMP to further prove its selectivity.

5.3.1. Phosphodiesterase inhibitory activity

PDE activity was measured using an adaptation of the IMAP1 fluorescence polarization phosphodiesterase assay (Molecular Devices, Sunnyvale, CA, USA). PDE hydrolysis of the fluorescent-labelled substrate allows it to bind the IMAP1 reagent, which increases fluorescence polarization (FP). The assay used fluorescein (Fl)-cAMP and tetramethylrhodamine (TAMRA)-cGMP as substrates. The different excitation and emission spectra of the substrates (485–530 nm for Fl and 530–590 nm for TAMRA) allowed for simultaneous measurement of cAMP and cGMP hydrolysis in the same well. The assays were performed in 96-well microtiter plates using a reaction buffer containing 10 mM Tris-HCl (pH 7.2), 10 mM MgCl₂, 0.05% NaN₃ and 0.1% phosphate-free bovine serum albumin as the carrier. Each well contained 20 μL of recombinant enzyme (BPS Biosciences, San Diego, CA, USA) and 10 μL inhibitor. The reaction was initiated by the addition of 10 μL of a substrate solution containing 50 nM Fl-cAMP and/or TAMRA-cGMP. After incubating at room temperature for 60 min the reaction was terminated by adding 120 μL of binding solution. FP was measured with a BioTek Synergy 4 (BioTek Instruments, Winooski, VM, USA) [39].

5.4. Molecular modelling

General procedures. Inhibitors were designed, built and energy minimized with MOE using the semi-empirical Hamiltonian AM1.

5.4.1. Clustering

23 structures were retrieved from the PDB database and superimposed with MOE based on their backbone atoms (for X-rays present as dimer or trimer all monomers were superimposed). Consensus clustering was performed with MOE and the most representative structures retained to form a small meaningful ensemble to be used in docking experiments.

5.4.2. Homology modelling

A set of 10 models was generated using modeler 9V8 [40,41] with PDB 3BJC and residues 790–809 (M-loop) of 2H42 as templates. Crystal structures were previously superimposed. The default all-hydrogen-model python script was used. Best model according to modeler 9V8 internal DOPE score was selected.

5.4.3. Docking

Compound **I**, the metal ions Zn²⁺ and Mg²⁺ as well as the three water molecules close to the piperazinedione carbonyl oxygen of **I**

were merged from 1XOZ into PDB 3BJC, 2H42 and 2H44 after superimposition. These newly generated complexes were refined using the LigX module of MOE. A force constant of 1 kcal/mol was used to restrain the C_α atoms of the protein, the ligand and the water molecules. The refined and superposed complexes were used in the ensemble docking.

Ensemble docking was performed using the docking software GOLDv5.0 and the GOLDScore (GS) fitness function [34,35]. The refined structures 1XOZ, 3BJC, 2H42 and 2H44 were used as representative ensemble. The active site was set by including all residues within 9 Å of compound **I**. Each compound of the small subset (**I**, **29**, **30**) was docked 50 times and the top 10 ranked poses retained.

Multiple single conformer docking was performed using AutoDock Vina v1.1.2 [36]. The same four complexes as for the ensemble docking were used with a set of 25 compounds (**I**, **1**, **4**, **5**, **8**, **9**, **11**, **12**, **13**, **14**, **15**, **16**, **17**, **18**, **20**, **21**, **25**, **26**, **29**, **30**, **33**, **34**, **35**, **36**, **37**), however with stripped metal ions Zn²⁺ and Mg²⁺. The docking parameters were kept to their default values. However, exhaustiveness was set to 30. The size of the docking grid was 27 Å × 25 Å × 27 Å, which encompassed the entire PDE5 active site, and centred close to Phe820.

Appendix A. Supplementary data

Supplementary data related to this article can be found at <http://dx.doi.org/10.1016/j.ejmech.2012.09.029>.

References

- [1] J.A. Beavo, L.L. Brunton, Nat. Rev. Mol. Cell. Biol. 3 (2002) 710.
- [2] A.L. Burnett, Am. J. Cardiol. 96 (2005) 29M.
- [3] T.W. Rall, E.W. Sutherland, J. Biol. Chem. 232 (1958) 1065.
- [4] R.W. Butcher, E.W. Sutherland, J. Biol. Chem. 237 (1962) 9021.
- [5] J.A. Beavo, Physiol. Rev. 75 (1995) 725.
- [6] J.D. Corbin, S.H. Francis, J. Biol. Chem. 274 (1999) 13729.
- [7] J.D. Corbin, S.H. Francis, Int. J. Clin. Pract. 56 (2002) 453.
- [8] Z. Sui, Expert Opin. Ther. Patents 13 (2003) 1373.
- [9] A. Daugan, P. Grondin, C. Ruault, A.C. Le Monnier de Gouville, H. Coste, J.M. Linget, J. Kirilovsky, F. Hyafil, R. Labaudiniere, J. Med. Chem. 46 (2003) 4523.
- [10] A. Daugan, P. Grondin, C. Ruault, A.C. Le Monnier de Gouville, H. Coste, J.M. Linget, J. Kirilovsky, F. Hyafil, R. Labaudiniere, J. Med. Chem. 46 (2003) 4533.
- [11] R.C. Kukreja, R. Ockaili, F. Salloum, Y. Chang, J. Hawkins, A. Das, L. Xi, J. Mol. Cell. Cardiol. 36 (2004) 165.
- [12] J. Prickaerts, A. Sik, W.C.G. van Staveren, G. Koopmans, H.W.M. Steinbusch, F.J. van der Staay, J. de Vente, A. Blokland, Neurochem. Int. 45 (2004) 915.
- [13] S. Hood, M. Kirby, Br. J. Diabet. Vas. Dis. 4 (2004) 383.
- [14] J.D. Whitt, N. Li, H.N. Tinsley, X. Chen, W. Zhang, Y. Li, B.D. Gary, A.B. Keeton, Y. Xi, A.H. Abadi, W.E. Grizzle, G.A. Piazza, Cancer Prev. Res. (Phila) 5 (2012) 822.
- [15] P. Serafini, K. Meckel, M. Kelso, K. Noonan, J. Califano, W. Koch, L. Dolcetti, V. Bronte, I. Borrello, J. Exp. Med. 203 (2006) 2691.
- [16] G. Cheng, H. Wang, H. Robinson, J. Cai, H. Ke, Biochem. Pharmacol. 75 (2008) 1717.
- [17] Y.H. Jeon, Y.S. Heo, C.M. Kim, Y.L. Hyun, T.G. Lee, S. Ro, J.M. Cho, Cell. Mol. Life Sci. 62 (2005) 1198.
- [18] G.L. Card, B.P. England, Y. Suzuki, D. Fong, B. Powell, B. Lee, C. Luu, M. Tabrizid, S. Gillette, P.N. Ibrahim, D.R. Artis, G. Bollag, M.V. Milburn, S.H. Kim, J. Schlessinger, K.Y. Zhang, Structure 12 (2004) 2233.
- [19] B.J. Sung, K.Y. Hwang, Y.H. Jeon, J.L. Lee, Y.S. Heo, J.H. Kim, J.M. Yoon, Y.L. Hyun, E. Kim, S.J. Eum, S.Y. Park, J.O. Lee, T.G. Lee, S. Ro, J.M. Cho, Nature 425 (2003) 98.
- [20] H. Wang, Y. Liu, Q. Huai, J. Cai, R. Zoraghi, S.H. Francis, J.D. Corbin, H. Robinson, Z. Xin, G. Lin, H. Ke, J. Biol. Chem. 281 (2006) 21469.
- [21] R. Zoraghi, S.H. Francis, J.D. Corbin, Biochemistry 46 (2007) 13554.
- [22] A.H. Abadi, B.D. Gary, H.N. Tinsley, G.A. Piazza, M. Abdel-Halim, Eur. J. Med. Chem. 45 (2010) 1278.
- [23] N.S. Ahmed, B.D. Gary, G.A. Piazza, H.N. Tinsley, S. Laufer, A.H. Abadi, J. Med. Chem. 6 (2010) 374.
- [24] H.A. Mohamed, N.R. Girgis, R. Wilcken, M. Bauer, H.N. Tinsley, B.D. Gary, G.A. Piazza, F.M. Boeckler, A.H. Abadi, J. Med. Chem. 54 (2011) 495.
- [25] N.S. Ahmed, B.D. Gary, H.N. Tinsley, G.A. Piazza, S. Laufer, A.H. Abadi, Arch. Pharm. (Weinheim) 344 (2011) 149.

- [26] T. Beghyn, C. Hounsou, B.P. Deprez, *Bioorg. Med. Chem. Lett.* 17 (2007) 789.
- [27] H.M. Berman, J. Westbrook, Z. Feng, G. Gilliland, T.N. Bhat, H. Weissig, I.N. Shindyalov, P.E. Bourne, *Nucleic Acids Res.* 28 (2000) 235.
- [28] G. Bottegoni, W. Rocchia, M. Rueda, R. Abagyan, A. Cavalli [Online], *PLoS ONE* 6 (2011) e18845.
- [29] M. Negri, M. Recanatini, R.W. Hartmann, *J. Comput. Aided Mol. Des.* 25 (2011) 795.
- [30] S.Y. Huang, X. Zou, *Proteins* 66 (2007) 399.
- [31] M. Rueda, G. Bottegoni, R. Abagyan, *J. Chem. Inf. Model.* 50 (2010) 186.
- [32] X. Barril, S.D. Morley, *J. Med. Chem.* 48 (2005) 4432.
- [33] G. Jones, P. Willett, R.C. Glen, A.R. Leach, R. Taylor, *J. Mol. Biol.* 267 (1997) 727.
- [34] M.L. Verdonk, J.C. Cole, M.J. Hartshorn, C.W. Murray, R.D. Taylor, *Proteins* 52 (2003) 609.
- [35] O. Trott, A.J. Olson, *J. Comp. Chem.* 31 (2010) 455.
- [36] L. Xiong, U. Zhan, *J. Comp. Chem.* 29 (2008) 1259.
- [37] B. Barren, L. Gakhar, H. Muradov, K.K. Boyd, S. Ramaswamy, N.O. Artemyev, *EMBO J.* 28 (2009) 3613.
- [38] Z. Xu, Z. Liu, T. Chen, T. Chen, Z. Wang, G. Tian, J. Shi, X. Wang, Y. Lu, X. Yan, G. Wang, H. Jiang, K. Chen, S. Wang, Y. Xu, J. Shen, W. Zhu, *J. Med. Chem.* 54 (2011) 5607.
- [39] W. Huang, Y. Zhang, J.R. Sportsman, *J. Biomol. Screen.* 7 (2002) 215.
- [40] A. Sali, T.L. Blundell, *J. Mol. Biol.* 234 (1993) 779.
- [41] A. Fiser, R.K. Do, A. Sali, *Protein Sci.* 9 (2000) 1753.